Advanced Muck-Pile Characterization: UAV, PCA and AI Synergy in Optimizing Blast Design and Excavator Loading Efficiency

Shrikant Krishnarao Titare[1], N. Sri Chandrahas[2*] , Yewuhalashet Fissha [3,4*], Mohammed Inayathulla [5] , Esma Kahraman [6]

[1] Geotechnical Engineering, Shri Ramdeobaba College of Engineering and Management, Nagpur, 440013, 7 India. shrikant8@gmail.com

[2] Mine Planning, GTS Limited, CKA Birla Group, Hyderabad, 500032, India. srichandru2009@gmail.com

[3] Department of Electrical and Computer Engineering, National Institute of Technology, Asahikawa College, 2-2-11 1-6 Syunkodai Asahikawa city Hokkaido 071-8142, Japan. yowagaye@gmail.com

[4] Department of Mining Engineering, Aksum University, 7080, Aksum, Tigray, Ethiopia.

[5] Gates Institute of Technology, Gooty, India. inayathulla512@gmail.com

[6]Department of Mining Engineering, Çukurova University, Adana 01250, Turkey

Abstract:

Muck-pile behavior plays a pivotal role in optimizing mining operations, as post-blast throw, drop, and lateral dispersion directly influence equipment selection and loading efficiency. The present study conducted a series of novel blasting trials to systematically evaluate the effects of different blast design parameters on key muck-pile characteristics. Principal Component Analysis (PCA) was employed to determine the most influential design variables for developing optimized blast configurations. The investigation comprised multiple combination blasts executed in four distinct phases at the OC1 RGIII mine of SCCL. Blast layouts were precisely developed using advanced blasting software and implemented in accordance with the parameters identified through PCA. Muck-pile properties were quantified using advanced AI-based analytical tools, yielding detailed and reliable insights.The findings revealed that a spacing-to-burden ratio of 1.35, stemming length equal to 0.9 times the burden, 1 m decking, and a V-pattern initiation sequence produced superior muck-pile conditions. This optimized configuration resulted in a reduction of drop by 3 m, a decrease in throw by 5.9 m, and an increased lateral spread of 19.3 m. These improvements contributed to smoother loader manoeuvrability, enhanced loading efficiency, and overall operational optimization.

Keywords: AI–Muckpile, Blast fragmentation, Muck-pile parameters and Unmanned Aerial Vehicle

1. Introduction

The fundamental aim of rock fragmentation in mining operations is to break the in-situ rock mass into manageable sizes. Drilling and blasting are the primary mechanisms responsible for producing fragmented material, and their effectiveness directly governs the productivity of downstream activities as well as the overall cost of mine production [1]. Beyond achieving the desired fragment size, muckpile characteristics such as throw, drop, and lateral dispersion play a crucial role in selecting suitable excavation equipment for bench operations.

During blasting, the detonation of explosives generates high-intensity stress waves that propagate through the rock mass [2]. These stress waves initiate and extend fractures, breaking the rock into smaller fragments, while the released explosive energy controls the movement and final placement of the broken material [3]. The resulting geometry of the muck pile is influenced by multiple blast design parameters, including burden, spacing, stemming height, decking length, and the initiation sequence [4].

The dispersion mechanism explains the downward movement and spatial redistribution of blasted material by describing how rock fragments of varying size and shape are displaced and distributed throughout the blast area. Furthermore, geological features such as bench-level joints and discontinuities can significantly modify fragmentation indices, including throw, drop, and lateral spread [5], as illustrated in Figure 1.

Fragmentation quality and its spatial arrangement have a direct impact on subsequent mining processes such as hauling and crushing. Well-distributed blasted material enhances operational efficiency, reduces production costs, and enables the expansion of loading zones [6]. Numerous studies have introduced statistical and soft-computing approaches—including regression analysis and fuzzy inference systems—to predict fragmentation outcomes based on blast parameters like burden, spacing, stemming length, charge per delay, and rock mass properties. These models have demonstrated improved predictive capability over conventional empirical methods [7]. Adapting blast designs to local geological conditions and spatial constraints is therefore essential for improving loading equipment performance [7].

Previous investigations into fragment size distribution have focused on its relationship with excavator productivity and maintenance requirements. These studies emphasize that fragmentation should be tailored to match excavator bucket capacity, allowing faster loading cycles and increased material handling efficiency. Achieving appropriate fragmentation and favorable muck-pile geometry is also critical for maximizing effective operating hours of excavation equipment [1].

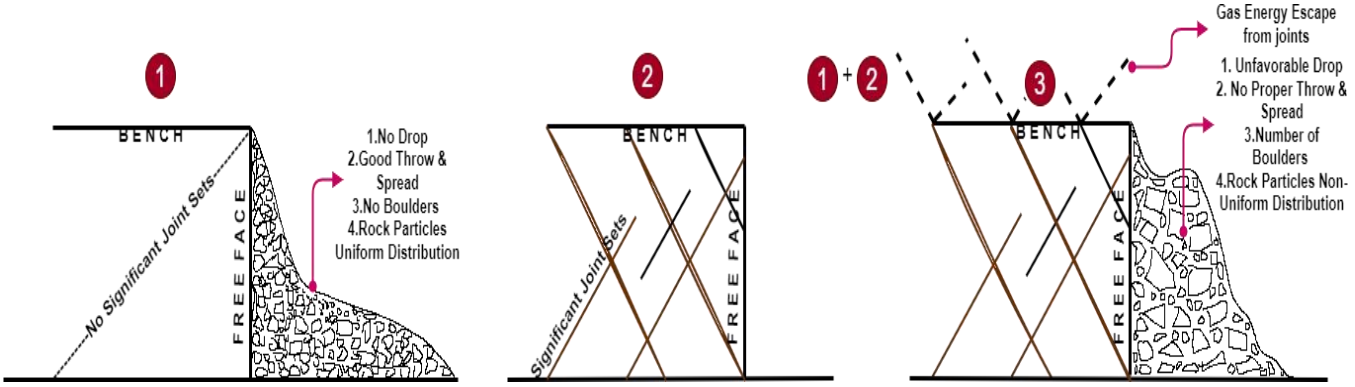

Figure 1. Impact of joints on rock fragmentation and muck pile characteristics

2. Literature review

As a result, blast pattern design must account for a range of influencing factors, including burden, spacing, blast-hole depth, stemming length, decking configuration, geological discontinuities, and firing sequence [8–12]. Among these, accurate burden determination is particularly critical, as commonly used empirical equations often exhibit considerable uncertainty [13]. Rock mass characteristics—such as joint orientation, spacing, and persistence—strongly influence muck-pile behavior [14, 15]. The complex interactions between geological conditions and controllable blast parameters governing muck-pile throw, drop, and spread have limited the practical applicability of existing empirical relationships and mathematical models [16].

A muck pile is defined as the accumulation of broken rock generated as a result of blasting operations. Its characteristics are of critical importance in surface mining, as they have a direct bearing on operational performance and productivity [17–19]. Predicting muck-pile behavior is essential for planning subsequent excavation and material-handling activities. Fundamental attributes such as fragment size distribution, particle geometry, and degree of breakage strongly influence loading and hauling efficiency, fragmentation assessment, and overall ore recovery. Improving these properties is therefore key to refining blast designs and minimizing costs associated with material handling.

Moreover, irregularly shaped fragments tend to increase internal friction and reduce flowability, which can cause handling difficulties and accelerate wear on mining equipment.

Studies examining muck-pile drop, throw, and lateral spread during blasting have reported considerable variation arising from differences in rock mass characteristics, blast design parameters, environmental conditions, and explosive properties. Drop describes the vertical movement of blasted material and is governed by factors such as explosive type, blasthole depth, and geological structure [17]. Throw refers to the horizontal displacement of fragments and is primarily controlled by blast geometry and the distribution of explosive energy. Spread denotes the sideways extent of the muck pile and is affected by ground conditions, blast orientation, and the presence of physical barriers. Despite advances in blasting technology and analytical tools, precise prediction of muck-pile behavior remains complex, underscoring the need for continued research and robust field data to enhance safety, operational efficiency, and sustainable blasting practices [21].

2.1 Review of muck pile sciences in relation to excavator selection, and blast design parameter

Muck pile science is an interdisciplinary area of research that examines the physical and spatial characteristics of blasted rock produced during mining operations. A comprehensive understanding of muck pile behavior is essential for selecting appropriate excavation equipment and achieving efficient material handling [21]. Characteristics such as fragment size, particle geometry, and degree of breakage have a direct impact on excavator productivity. For instance, muck piles composed of coarse, angular fragments generally demand excavators with higher breakout forces and larger bucket capacities to enable effective loading [1]. In contrast, finer and more uniformly fragmented muck piles are better handled using smaller buckets, which can improve cycle times and operational efficiency. Incorporating muck pile analysis into equipment selection strategies allows mining operations to enhance productivity while minimizing costs associated with inefficient loading practices.

Numerous investigations have explored the interaction between muck pile properties, excavator performance, and blast design variables. Zhang et al. [21], for example, analyzed the influence of blast design parameters on fragmentation behavior in an open-pit mine. Their study demonstrated that changes in explosive charge distribution significantly altered both the size distribution and morphology of muck piles. An increase in the spacing-to-burden ratio was found to reduce fragment size while producing irregular muck pile geometries in terms of throw, drop, and spread [21]. This effect is attributed to the reduction in effective burden and the relative increase in spacing caused by explosive initiation dynamics [22]. The combination of increased spacing and reduced burden resulted in the formation of thin rock sections, leading to less favorable fragmentation. Optimal spacing-to-burden ratios were identified as 1.15 for staggered patterns and 1.25 for rectangular patterns, while commonly applied ratios typically range between 1 and 2. In general, spacing-to-burden ratios between 1.1 and 1.3 are considered most effective for achieving desirable fragmentation and facilitating efficient excavator selection [23].

The firing pattern governs the sequence and direction of detonation energy transfer between blastholes, guiding stress wave propagation throughout the rock mass. A key objective of firing design is the progressive creation of free faces, which enables controlled rock movement during blasting [24]. By directing subsequent rows of blast holes toward newly created free faces, firing patterns play a decisive role in shaping muck pile displacement. In addition, previous research has

shown that decking configuration substantially influences rock movement, particularly in jointed rock masses, thereby affecting final muck pile geometry [25].

Muck pile formation varies significantly depending on the structural condition of the rock mass. Jointed benches contain natural fractures and discontinuities, whereas non-jointed benches exhibit relatively intact rock structures. Distinguishing between these conditions is critical for effective blast design and material handling strategies [26]. Studies have reported that blasting in jointed benches often produces larger fragments and more irregularly shaped muck piles compared to non-jointed conditions [27]. Joints act as preferential stress-release pathways, leading to uneven fracture development and increased fragment size. The intensity and orientation of jointing strongly influence both fragmentation patterns and overall blasting safety [28]. Moreover, joint orientation affects fracture propagation paths and stress concentration, ultimately controlling muck pile shape and distribution [29].

Additional investigations have examined the influence of joint spacing on muck pile characteristics in open-pit environments. Results indicate that closely spaced joints promote greater crack propagation and finer fragmentation within muck piles, emphasizing the importance of accounting for joint spacing in blast design optimization [30–31]. Similarly, studies focusing on joint plane orientation in coal mining environments revealed that changes in joint orientation significantly affect fragment size distribution and particle morphology, reinforcing the necessity of incorporating both joint and bedding plane information into blast design processes [32]. Fragmentation quality was observed to decline when shock waves intersected joint planes at oblique angles, whereas improved fragmentation occurred when blast energy propagated parallel to planes of weakness. Aligning the free face parallel to dominant joint planes was found to enhance fragmentation and improve overall muck pile configuration in many cases [33].

The efficiency of downstream operations such as loading, hauling, and crushing in surface mines is largely governed by the fragmentation and spatial distribution of blasted material. Consequently, reliable prediction of muck pile characteristics prior to blasting is essential for achieving operational efficiency and cost control [34–38]. Previous studies have assessed the influence of parameters including spacing-to-burden ratio, stemming length, decking configuration, firing sequence, explosive charge, and joint conditions. A strong correlation between joint presence and the outcomes of successive blasting operations has been consistently reported in the literature [39, 40].

While recent research has explored UAV- and AI-assisted approaches for blast analysis, the present study offers several novel contributions. These include: (i) analysis of a large-scale industrial dataset comprising 164 production blasts conducted under varying joint conditions; (ii) application of Principal Component Analysis (PCA) to systematically identify and optimize controllable blast design parameters; and (iii) identification of a unique and effective blast configuration involving V-pattern initiation, a spacing-to-burden ratio of 1.35, and 1 m decking, which significantly enhances lateral muck pile spread while reducing drop. This optimized configuration enables improved loader maneuverability and higher loading efficiency. Overall, this study advances existing knowledge by providing statistically validated and practical guidelines for blast design in jointed bench environments.

3. Field data collection

The experimental investigations were carried out at Opencast Mine I, Ramagundam, KLM Limestone Mine, and Kesoram Limestone Mine, all operated by Singareni Collieries Company Limited (SCCL) within the South Godavari Basin of Telangana, as shown in Figures 3(a) and 3(b). The study sites are geographically located between latitudes 18°39′07″ N and 18°41′05″ N, and longitudes 79°32′37″ E and 79°33′53″ E. The mining region is characterized by a substantial overburden comprising thick deposits of soil, alluvium, and sandy layers, underlain by rock units of the Barakar Formation belonging to the Lower Gondwana Group.

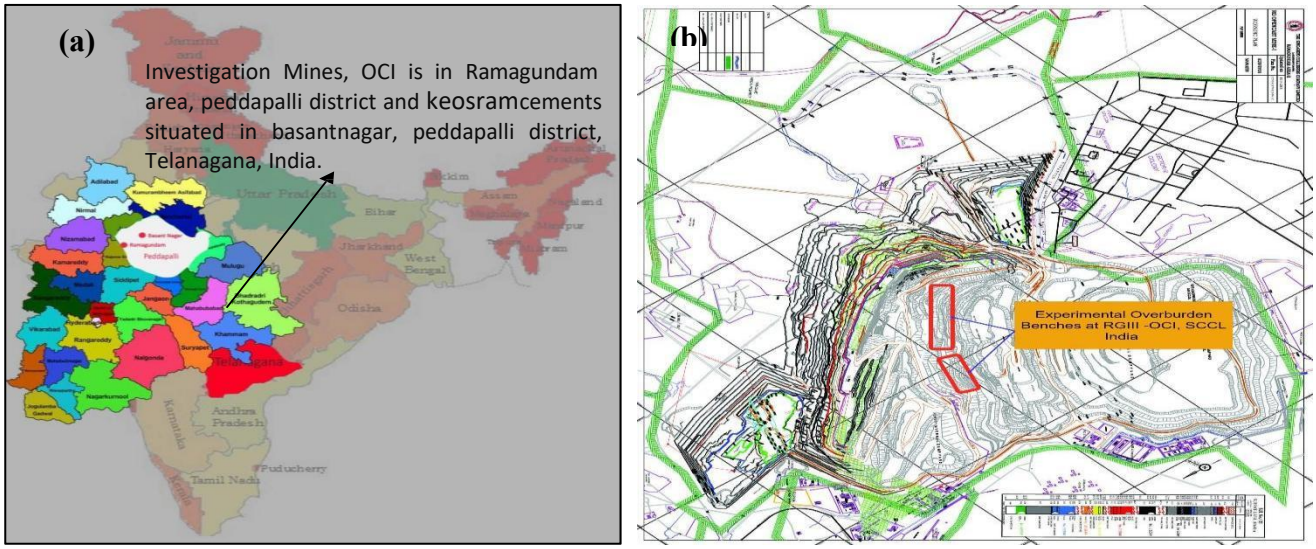

Figure 3. (a) Location of experiment sites on India Map, (b) Surface plan of OCI, SCCL.

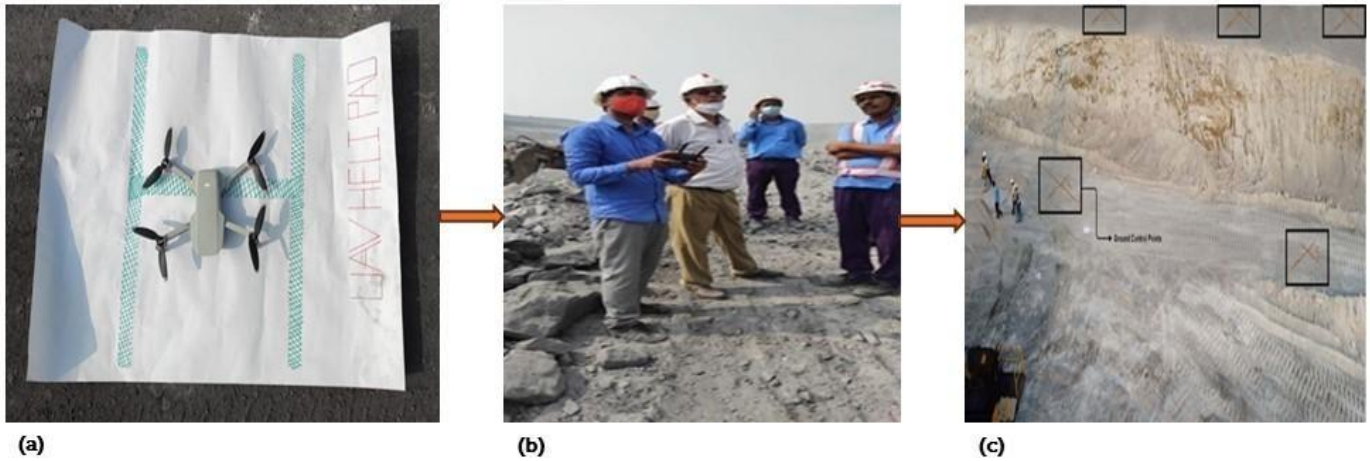

Figure 4. (a) Drone Helipad with DJI MAVIC DRONE at OCI Mine, Ramagundam Region, (b) DJI MAVIC Drone flying at OC I, RGIII SCCL to capture bench photographs, (c) GCP showing on bench top and floor at OCI Singareni Collieries Company Limited (SCCL), Ramagundam region to create 3D model for designing blasts.

A DJI Mavic unmanned aerial vehicle (UAV) was utilized for image acquisition in the present study, offering both high-resolution photography and video recording at 4K quality. The UAV has a lightweight structure of 258 g and a maximum flight endurance of approximately 25 minutes per battery cycle. Prior to deployment, signal calibration was carried out to eliminate connectivity issues and ensure stable flight operation. Figures 4(a) and 4(b) present aerial views of the limestone blast site captured during the survey.

The UAV was deployed to obtain orthogonal images of the bench surfaces before and after blasting. The primary aim of the aerial survey was to collect detailed visual data on joint orientation, spacing, and persistence along the vertical face of the bench. During data acquisition, the UAV was flown at an altitude of 30.48 m above the blast zone, maintaining an image overlap of approximately 75% to ensure sufficient coverage for photogrammetric reconstruction.

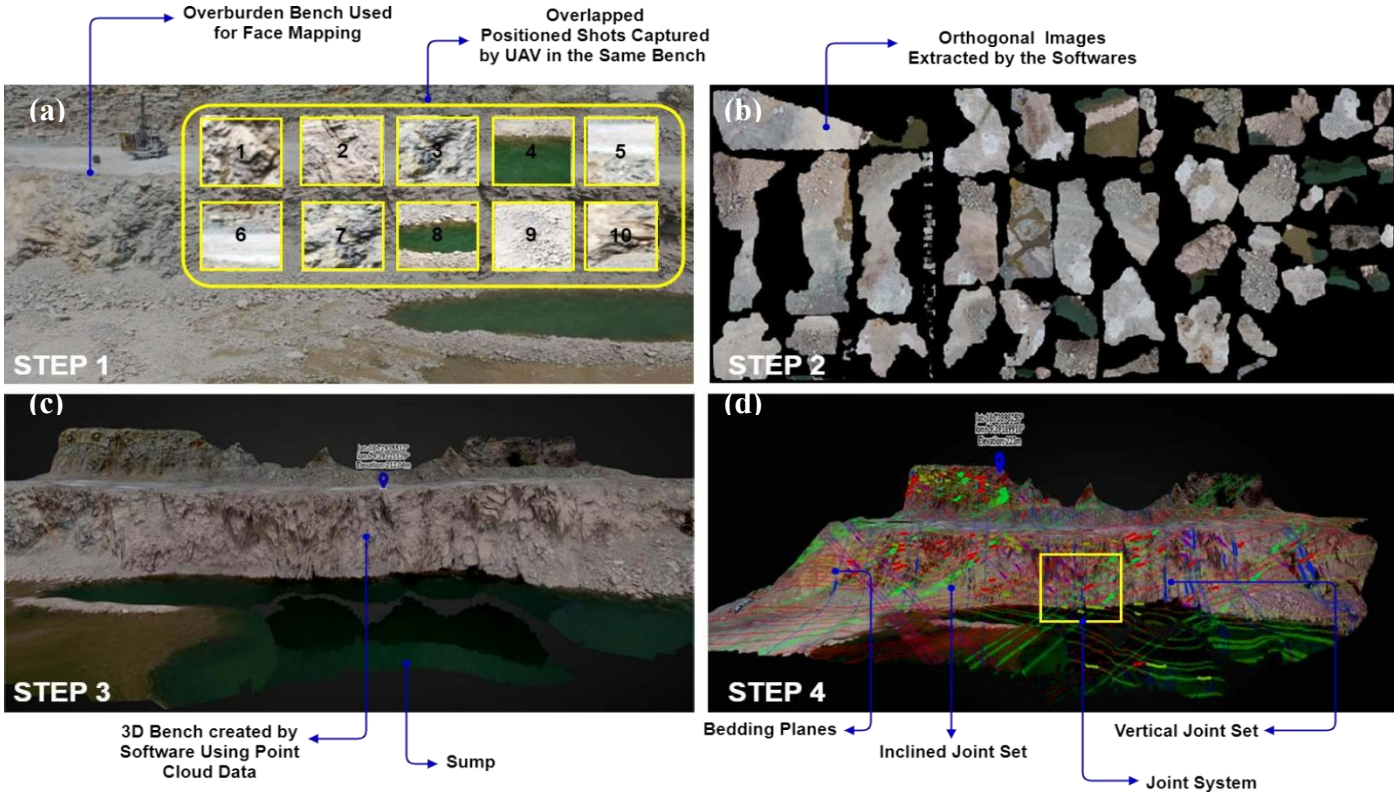

Figure 5. (a) Systematic representation of overlapping photos shot of UAV at OCI Mine, Ramagundam Region, (b) Ortho-sectional images extracted by software, (c) 3D Model created by software using point cloud data, (d) Systematic bench 3D Model representation with joint sets.

To achieve high-quality imagery, the camera tilt angle was adjusted between 30° and 45°, enabling clear visualization of both the bench crest and the bench floor. Accurate three-dimensional modeling for geologically representative blast design requires careful selection of the image acquisition direction. Accordingly, the bench face was segmented into three zones—upper section, lower section, and a combined crest–toe section—allowing image overlaps in the range of 70–80%. The UAV-acquired images were subsequently processed using STRAYOS software to generate rock mass models. Figure 5(a–d) illustrates the complete workflow, from UAV data capture to the interpretation of rock mass conditions using the reconstructed 3D model.

Ground control points (GCPs) were established to define blast site locations and improve model accuracy. For each 3D model, four to five GCPs were marked on the ground using high-contrast red identifiers, as shown in Figure 4(c). Additional GCPs were placed at the outer boundaries of each site to enhance spatial coverage. Since placing GCPs on fragmented muck piles is challenging, at least one control point was assigned at each elevation level, including the muck pile surface. Throughout the survey, the UAV was operated in a manner similar to a conventional fixed-wing aircraft, ensuring stable and consistent flight paths.

During data acquisition, ground control point (GCP) markers were carefully retrieved, image distortion was minimized, and consistent camera focus was maintained throughout the flight. Following the targeted UAV surveys, GCP information was integrated into the processing software to enable the generation of accurate three-dimensional models of the blast benches.

The GCP dataset was prepared using the geographic coordinates (latitude and longitude) of each control point referenced to the EPSG coordinate system. The data were processed using EPSG 32644 and imported into STRAYOS software in CSV format along with the corresponding UAV imagery. After uploading, the software interface displayed the GCP locations superimposed on satellite images, allowing for visual verification and precise adjustment of control point positions, as illustrated in Figure 5. The ground sampling distance for the generated models was maintained at 0.49 cm per pixel.

3.1. Joint planes analysis

To assess the joint intensity and patterns of the target bench, the Rock Mass AI Strayos software, which utilizes artificial intelligence (AI), was employed. The software's underlying algorithm is ally designed to analyze data collections for features associated with rock joints. Images of rock joints are processed multiple times to identify distinct patterns within the gathered image data. Figure 5(d) displays the three joint sets clustered during the plane analysis.

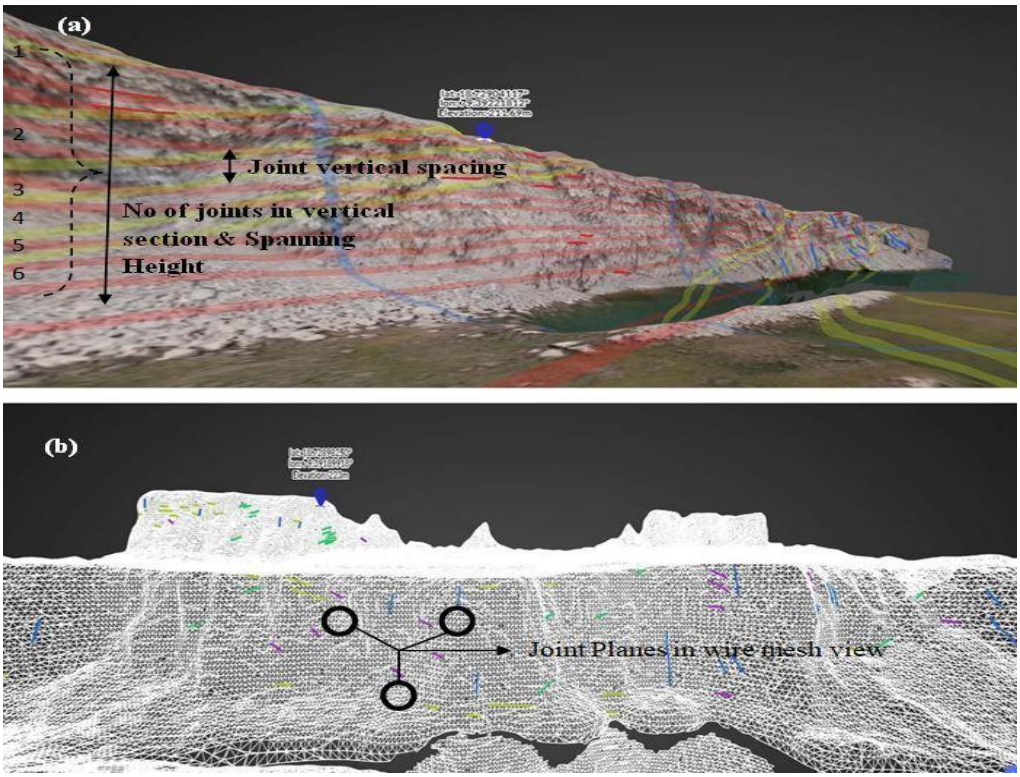

Figure 6. (a) Systematic view of joints in bench at OCI, RGIII, SCCL, (b) wire meshed model of bench at OCI, RGIII, SCCL.

The joint characterization study revealed that the rock mass at the Kesoram Limestone Mine is highly weathered and structurally non-uniform. Among the three experimental sites, this mine exhibited the greatest density of joint planes. Based on field observations and engineering judgment, users can specify the required number of joint clusters, along with the corresponding dip and strike orientations. These clusters are defined according to the number of joints intersecting the vertical bench section and the

vertical spacing of joints across the bench height, categorized into six classes (1–6). The identified joint planes and the corresponding wireframe representations are shown in Figures 6(a) and 6(b), while a summary of the results is provided in Table 2.

Table 2. Results of joint dip, strike directions and dip angle

Mine Name	No of benches	Bench Name	SET 1			SET 2			SET 3			SET 4			SET 5		
			D	S	DA	D	S	DA	D	S	DA	D	S	DA	D	S	DA
OPENCAST	03	1A SEAM	331	241	75	225	135	27	335	245	85	247	157	14	-	-	-
		2B SEAM	220	130	26	298	208	30	305	215	30	221	131	30	-	-	-
		3A SEAM	170	80	25	194	104	32	310	220	36	270	180	25	-	-	-
MINE – I OPENCAST MINE – II	03	1A TOP SEAM	310	220	81	312	222	17	190	100	20	231	141	65	-	-	-
		II SEAM	290	200	21	190	100	50	329	239	85	170	80	50	-	-	-
		3A SEAM	200	120	24	300	210	73	250	160	41	184	94	71	-	-	-
KESORAM LIMESTONE MINE	03	D BLOCK	180	90	18	170	80	30	170	80	20	306	216	36	237	147	20
		G BLOCK	319	229	78	320	230	70	310	220	69	231	141	72	212	122	38
		F BLOCK	194	104	48	247	157	28	247	157	21	200	120	28	173	83	40

D – DIP DIRECTION S – STRIKE DIRECTION DA – DIP ANGLE

It is recognized that the vertical joint spacing values derived through AI analysis correspond to the spacing of observable structural discontinuities along the exposed bench face, encompassing bedding planes, prominent joints, and persistent fractures, rather than representing only primary sedimentary layer thicknesses. Field validation demonstrated that these continuous discontinuities play a decisive role in controlling fracture development and subsequent muck-pile displacement.

3.2. Principle component analysis (PCA)

In this study, Principal Component Analysis (PCA) was performed using XLSTAT to evaluate the influence of both independent and dependent variables and to identify dominant trends for selecting the final blast design adopted in the experimental trials. The blast design parameters included in the analysis comprised hole diameter, burden, spacing, front-row burden, decking length, stemming length, firing pattern, average explosive charge per blast, and total explosive quantity. In addition, key geotechnical variables—namely joint spacing, joint aperture, joint orientation, number of joints, and joint persistence (spanning height)—were incorporated into the PCA.

The joint-related parameters used in the PCA were derived from artificial intelligence–based analysis software during the preliminary site investigation, as summarized in Table 2.

Interpretation of the PCA results was carried out using the correlation circle generated by XLSTAT, which serves as the primary basis for assessing variable relationships. The correlation circle enables visualization of the interactions between independent and dependent parameters and is interpreted in terms of three relational categories: positive, negative, and orthogonal correlations. Variables plotted close to each other within the same quadrant exhibit positive correlation, whereas variables positioned in opposite quadrants demonstrate negative correlation. Variables located approximately at right angles to one another are considered orthogonal, indicating little to no mutual influence. Positive correlations reflect directly proportional relationships, negative correlations indicate inverse relationships, and orthogonal positioning signifies independence between variables.

Using XLSTAT, relationships between dependent variables—specifically mean fragment size and peak particle velocity—and independent blast design parameters such as burden, spacing, front-row burden,

stemming length, decking length, hole depth, and explosive charge were systematically evaluated.
The PCA was applied to identify the degree of association and clustering among multiple parameters and observational datasets. Blasting performance is governed by the combined interaction of numerous factors, and analyses limited to individual variables fail to capture these complex interactions. Consequently, PCA provides an effective framework for comprehensively assessing blast fragmentation behavior and muck-pile characteristics by integrating multiple influencing parameters. The PCA results and parameter relationships are presented in Figure 7.

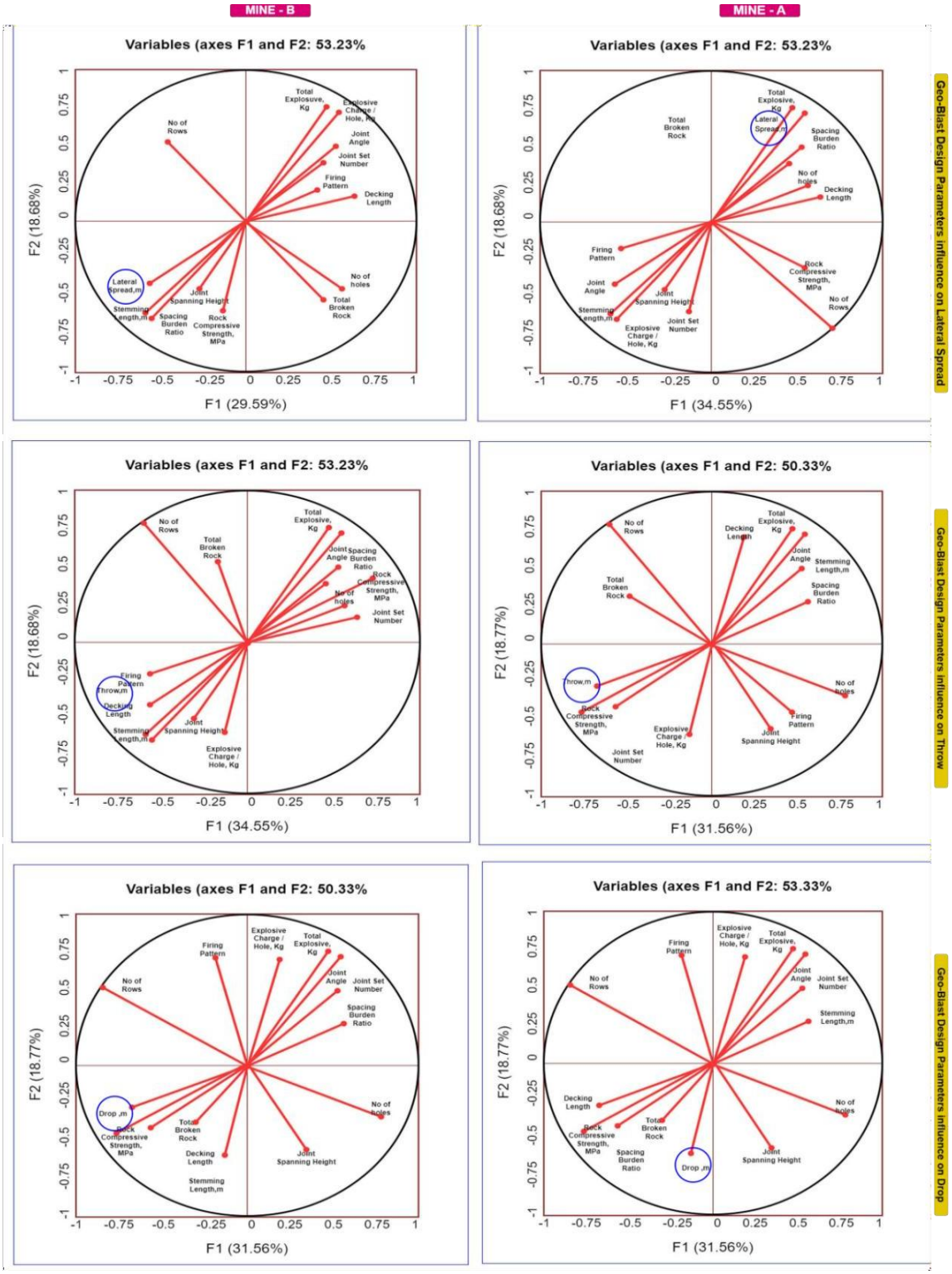

Figure 7. Throw, drop and lateral spread correlation circle diagram of mine A & Mine B

The PCA outcomes indicate that three principal components account for 82.4% of the overall data variability, with PC1 explaining 49.7%, PC2 contributing 21.3%, and PC3 representing 11.4% of the variance. The parameters exerting the greatest influence on muck-pile behavior were identified as spacing, burden, decking length, joint orientation, and total explosive energy. The firing pattern showed a strong loading on PC1 (0.78) and exhibited an inverse relationship with excessive muck-pile drop. Additionally, joint orientation and joint density demonstrated significant contributions to PC2, highlighting the dominant role of geological conditions in controlling lateral muck-pile spread (Table 3). With the exception of the number of rows, number of blast holes, uniaxial compressive strength of the rock, and total volume of rock fragmented, most baseline input variables showed either direct or inverse correlations with muck-pile characteristics.

A full-factorial experimental design was implemented based on the PCA findings. Three key parameters were selected as dominant factors: firing sequence (linear, diagonal, and V-pattern), spacing-to-burden ratio (1.20, 1.30, 1.35, and 1.40), and decking length (1.0 m, 1.5 m, and 2.0 m). To ensure statistical reliability across varying joint orientations, forty-two blast trials were conducted in each experimental phase (Table 3). Overall, the analysis comprised 164 production blasts as the primary dataset, supplemented by an additional 24 blasts used for validation to confirm the optimal ranges of the selected parameters

3.3. Blast design, prediction, and field experimentation

In alignment with the objectives of this investigation, each of the 32 blast designs was developed by accounting for the presence of joint planes, their dip–strike orientations, and the corresponding sectional uniaxial compressive strength of the rock mass, as identified through PCA-refined datasets. Charge distribution and decking lengths were systematically modified within STRAYOS software to simulate fragmentation behaviour and predict muck-pile geometry, as illustrated in Figure 10. The prediction framework within the software is based on the KUZRAM and SWEBREC fragmentation models.

The experimental program was structured into four distinct phases, designated as Phases I, II, III, and IV, as described below:

Phase I: All blast design parameters were kept constant, while the initiation pattern was varied in relation to joint orientation.

Phase II: All blast design parameters were held unchanged, except for the spacing-to-burden ratio, which was modified with respect to joint orientation.

Phase III: Blast geometry remained constant, while explosive charge and decking length were adjusted in accordance with variations in rock compressive strength.

Phase IV: Blast parameters were maintained except for the combined modification of firing pattern and spacing-to-burden ratio, implemented with reference to joint orientation.

For all mines included in the study, three initiation sequences—linear, diagonal, and V-pattern—were identified as the most frequently employed firing configurations. Consequently, all blast models were constructed using scaled representations of joint planes aligned with the dip and strike directions determined from geological assessments. These joint configurations were incorporated into the Rock

Mass AI module of STRAYOS software, with supporting information provided in Table 2 and Figure 5(d).

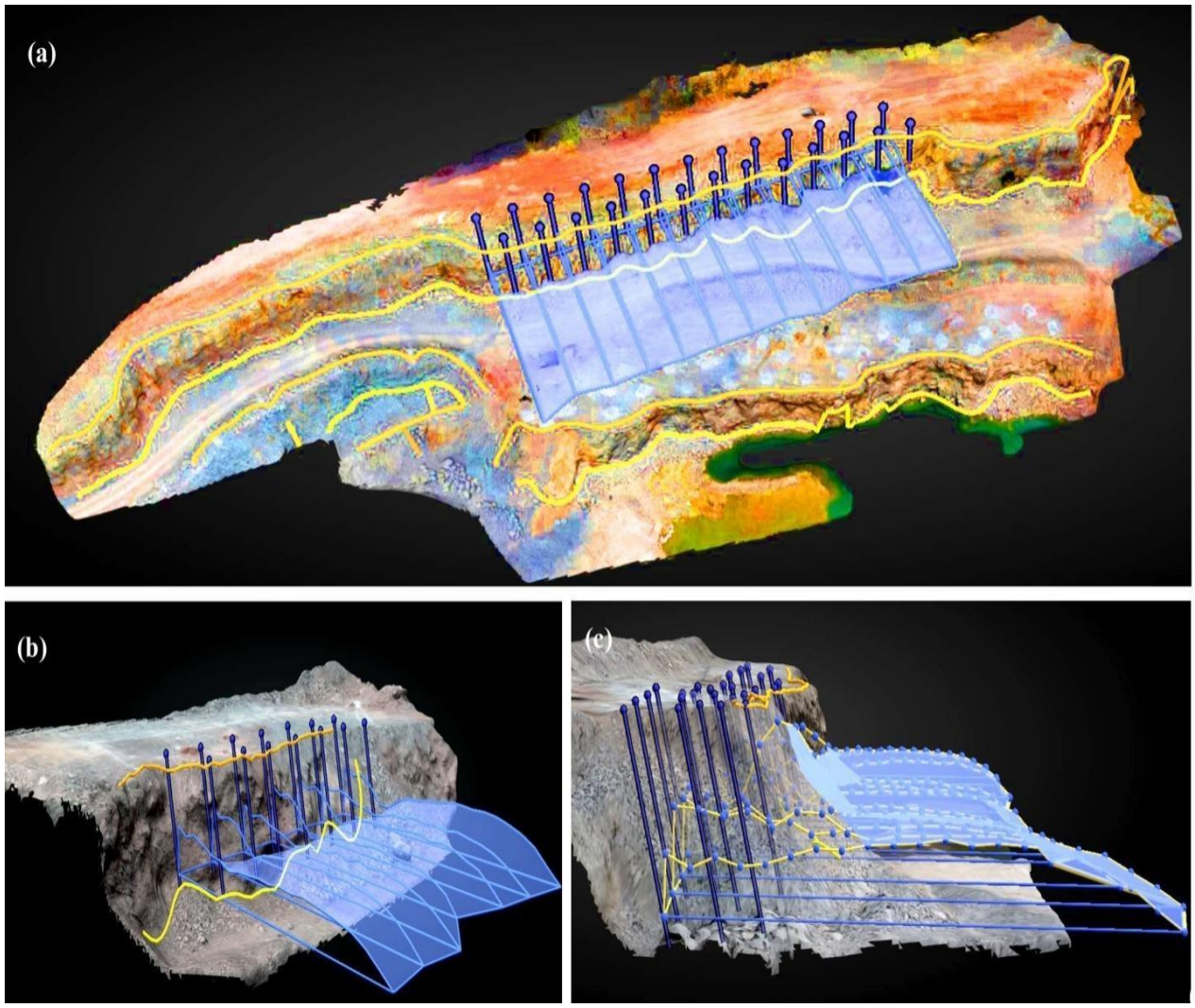

Figure 8. (a) Isometric view of 3D Model generated by software, (b) Isometric view of Muck-pile Prediction for respective blast design, (c) Cast analysis of muck pile prediction.

Beyond joint orientation and occurrence, joint frequency and joint persistence (spanning height) are critical considerations when determining burden and spacing. Incorporating these factors helps prevent the intersection of drill holes along joint planes, which can otherwise cause drill rod jamming and negatively affect blast economics. Throughout the experimental program, all blast parameters were held constant except for the variables under investigation, allowing a clear assessment of how different parameter combinations influenced fragmentation and muck-pile behavior. As a result, initiation accessories and delay sequencing were kept as uniform as possible across all blasts. Predicted muck-pile characteristics—including drop, throw, and lateral spread—along with corresponding excavator selection, are presented in Figures 8(b–c) and 10, while details of blast-hole charging and initiation layouts are shown in Figures 9(c–d).

A total of 164 production blasts were executed across two test sites over a 45-day period, with decking lengths adjusted to match variations in joint persistence. In coal mining operations, blasting was generally carried out using down-the-hole delays of 425 and 450 ms, hole-to-hole delays of 17 ms, and

row-to-row delays of 25 and 42 ms. V-pattern initiation was applied where required based on site-specific rock conditions, as illustrated in Figures 9(a–b). Site-mixed emulsion (SME) explosives were employed in conjunction with a booster–NONEL initiation system, whereas ANFO was used for limestone benches. Typically, two boosters were placed per meter of hole depth, and the average explosive consumption ranged between 45 and 55 kg per blast.

The stemming lengths adopted in this study (4.5–6.0 m) resulted in stemming-to-burden ratios exceeding the commonly recommended value of 0.67 for optimal fragmentation (Shukla et al., 2024). However, due to elevated bench heights and safety considerations, increased stemming was necessary to minimize flyrock hazards. The application of AI-optimized burden and spacing parameters, along with optimized firing patterns, effectively compensated for the higher stemming ratios, ensuring that fragmentation outcomes remained within acceptable operational limits.

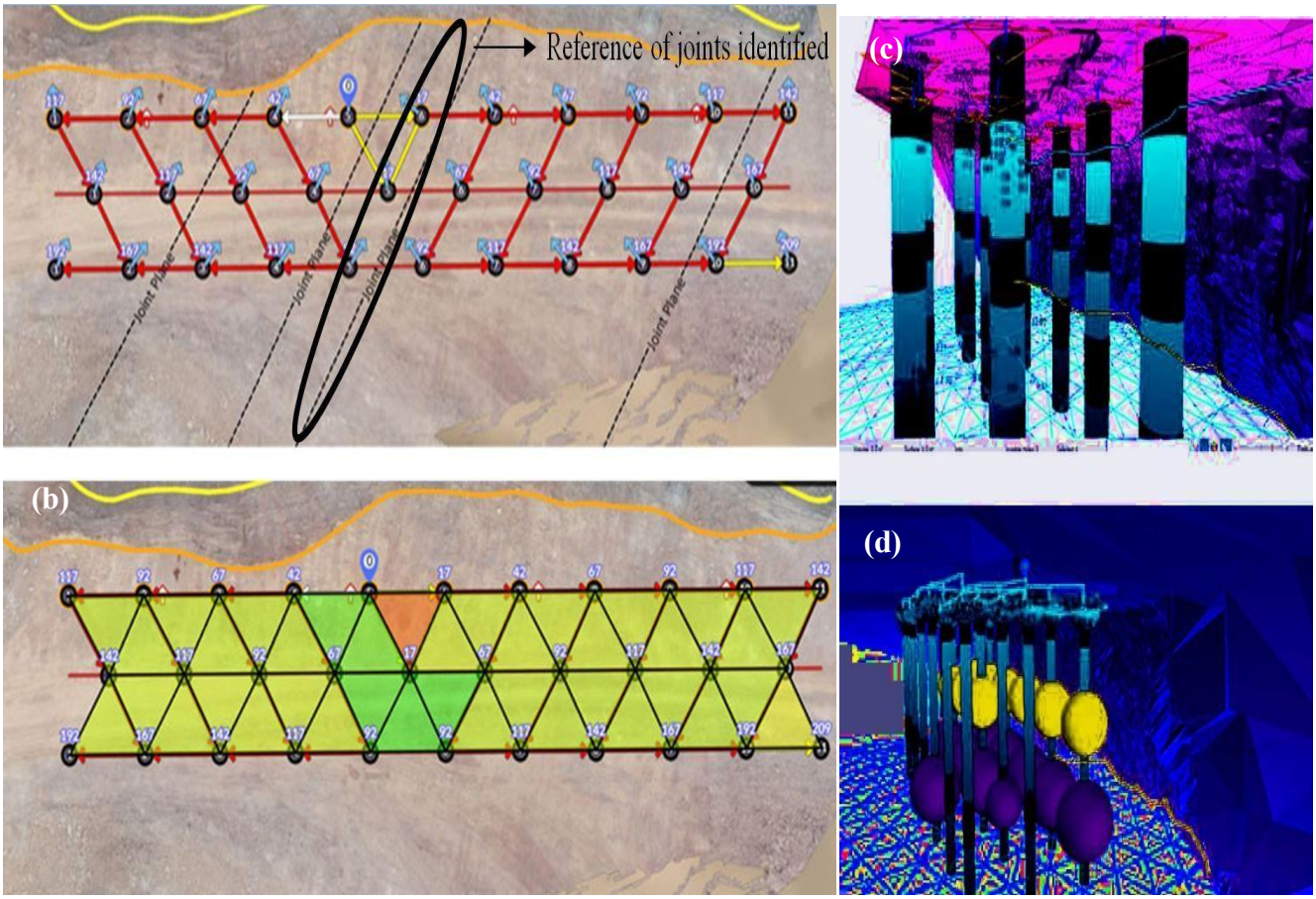

Figure 9. (a) V firing initiation flow and throw prediction of KLM site blats, Telangana, (b) Design of V firing pattern with joint references identified of KLM, Telanagana, (c) Blast hole charging interface, (d) Multi decking and initiation design and prediction in AI blasting software.

For the limestone bench trials, ANFO-charged blastholes typically contained an explosive load of approximately 18 kg per hole, supplemented with five to six boosters. All experimental blasts included in this investigation were carried out at OC-1 using site-mixed emulsion (SME) explosives. The SME density was controlled within the range of 1.25–1.29 g/cc during charging and subsequently reduced to 1.05–1.10 g/cc following a gassing period of 20–25 minutes.

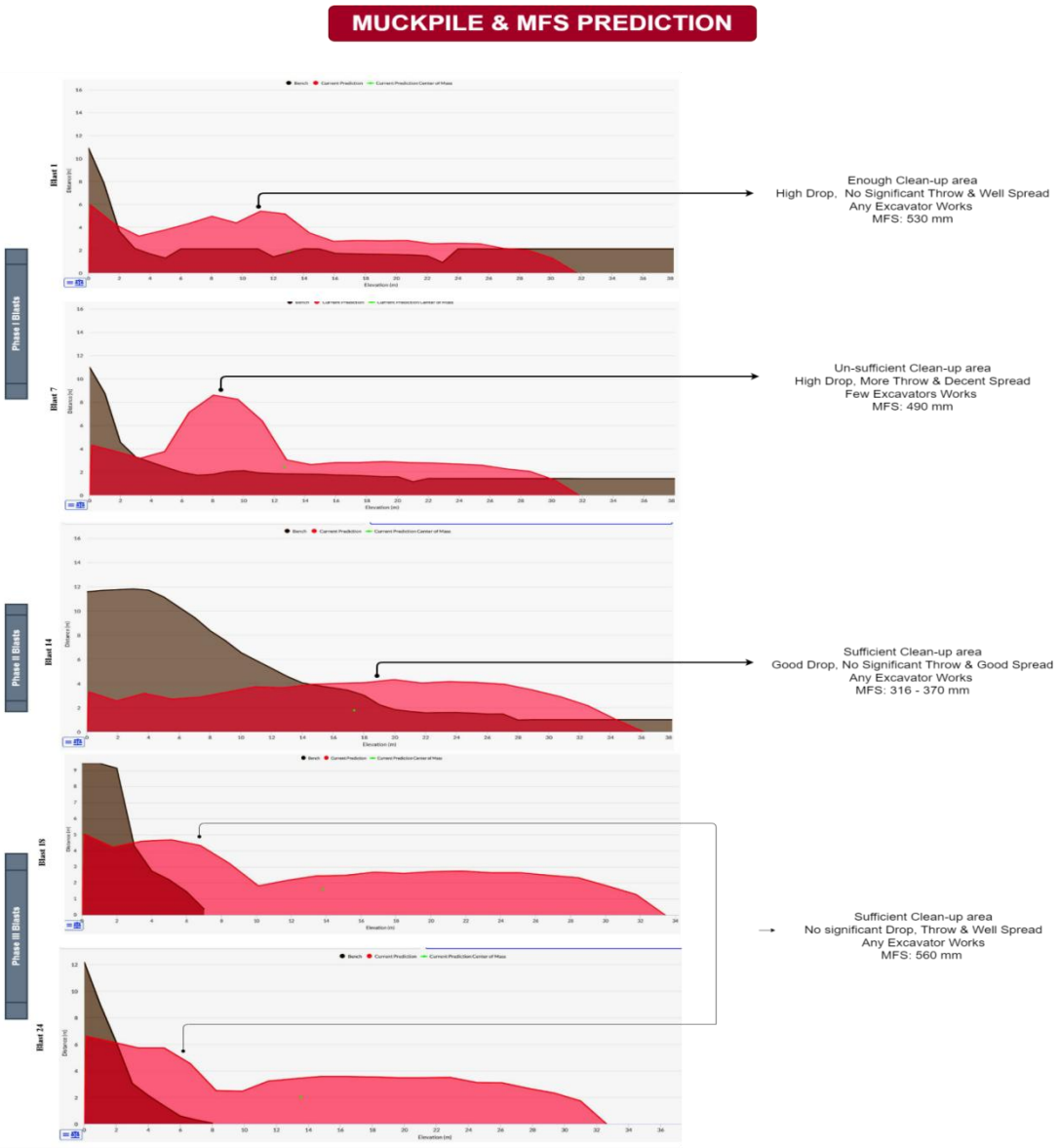

Figure 10. Muckpile characteristics Drop, Throw and lateral spread prediction in software, presented for few blasts to understand the trend and impact on the loader.

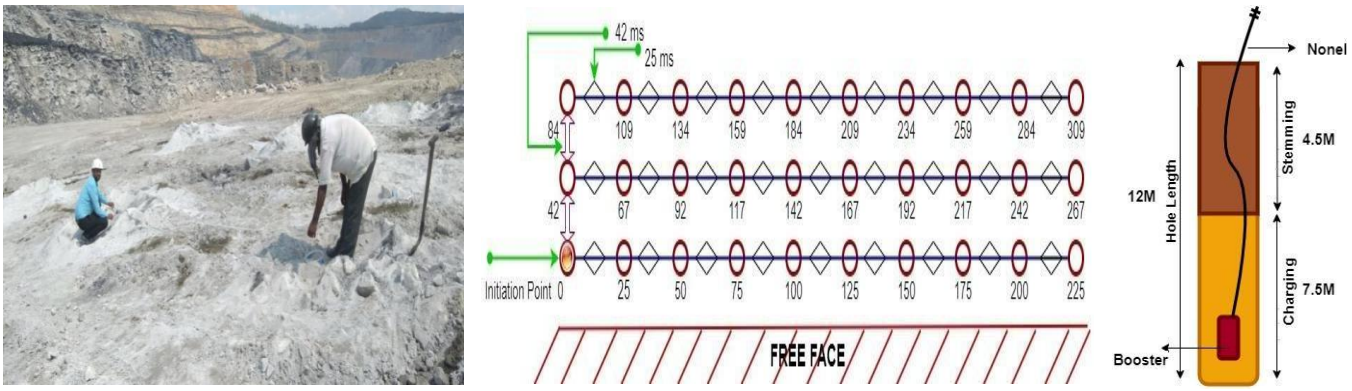

Figure 11. (a)Burden Spacing Measurement at OC1, RG3, SCCL, (b) Rectangular Drilling with Diagonal Firing Pattern at Mine, B Figure (c) Blast Hole Section at Mine.

Pentolite boosters were placed in each blasthole at approximately 0.2% of the total SME charge to improve

detonation efficiency and energy transmission. To achieve rapid and effective energy release, the viscosity of the SME was maintained between 40,000 and 80,000 cps. Representative field photographs and comprehensive blasting details are provided in Figures 11(a–c) and Table 3.

The considered St/B ≈ 1.6 -1.85 ratio is higher and contrast to general range of 0.6 to 0.9 of practicing. This is due to the presence of highly jointed overburden and limestone benches, the stemming column must counteract several rock-mechanics effects that invalidate the conventional St/B ratio. Joint planes, bedding surfaces, and persistent fractures create preferential gas-venting pathways, causing early loss of detonation gases and increasing flyrock risk along structural weaknesses. A longer stemming column provides the required confinement, maintaining borehole pressure long enough for fractures to propagate through the burden instead of venting prematurely through joints. Increasing stemming length therefore stabilizes gas pressure, promotes radial crack development, improves burden movement, and restricts uncontrolled ejection along weak planes. Therefore, in this study St/B > 1.8 was intentional and essential for safe energy confinement.

3.4. Fragmentation and muck-pile measurement

Rock fragmentation was assessed using high-resolution orthophotos and three-dimensional point clouds of the muck pile generated through UAV-based photogrammetry. These datasets were analyzed using Fragmentation AI software, which employs a U-Net–based convolutional neural network to perform both semantic and instance segmentation, enabling automatic identification and separation of individual rock fragments. Each detected fragment was geometrically approximated using a bounding rectangle, from which an equivalent mean particle diameter was calculated to establish the empirical particle size distribution (PSD).

The software subsequently derived key fragmentation indices, including D10, D50, and D80, and estimated the uniformity index (n), which governs the shape of the Kuz–Ram fragmentation curve. Fragmentation predictions using the KUZ–RAM model were generated by incorporating all necessary input parameters, such as rock factor (A), uniaxial compressive strength, joint spacing, number and orientation of discontinuities, burden, spacing, and specific charge. These inputs were obtained from AI-based joint characterization and field observations, as detailed in Section 3.1 and Table 2.

The experimentally measured PSD was further validated using both the classical KUZ–RAM model (Cunningham, 1987) and the SWEBREC distribution to ensure theoretical consistency. The resulting fragmentation curves and particle size measurements are illustrated in Figure 13.

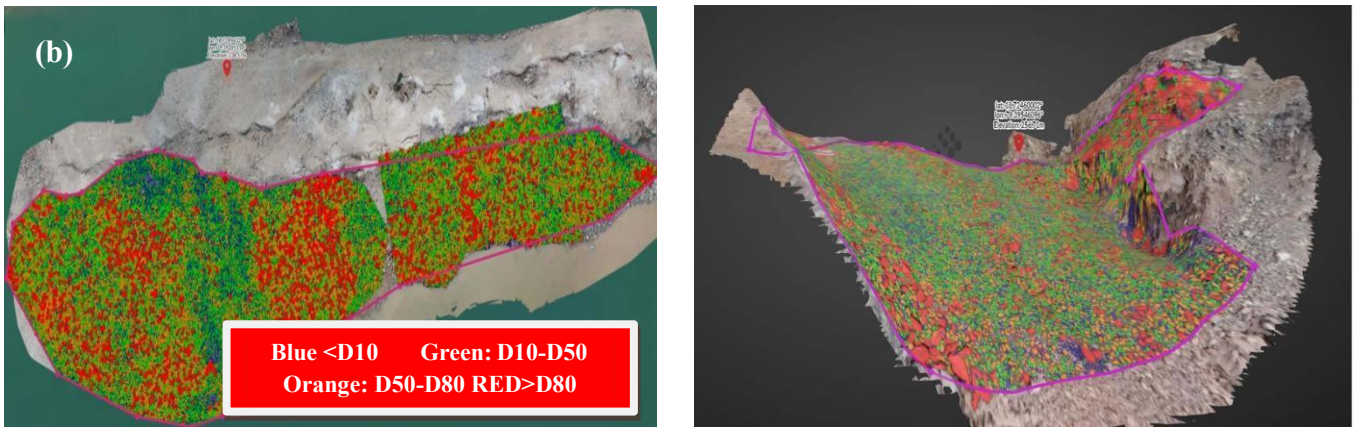

Figure 12. (a) Rock fragmentation analysis 3D MODEL in STRAYOS SOFTWARE, (b) Rock fragmentation analysis 2D MODEL in STRAYOS SOFTWARE.

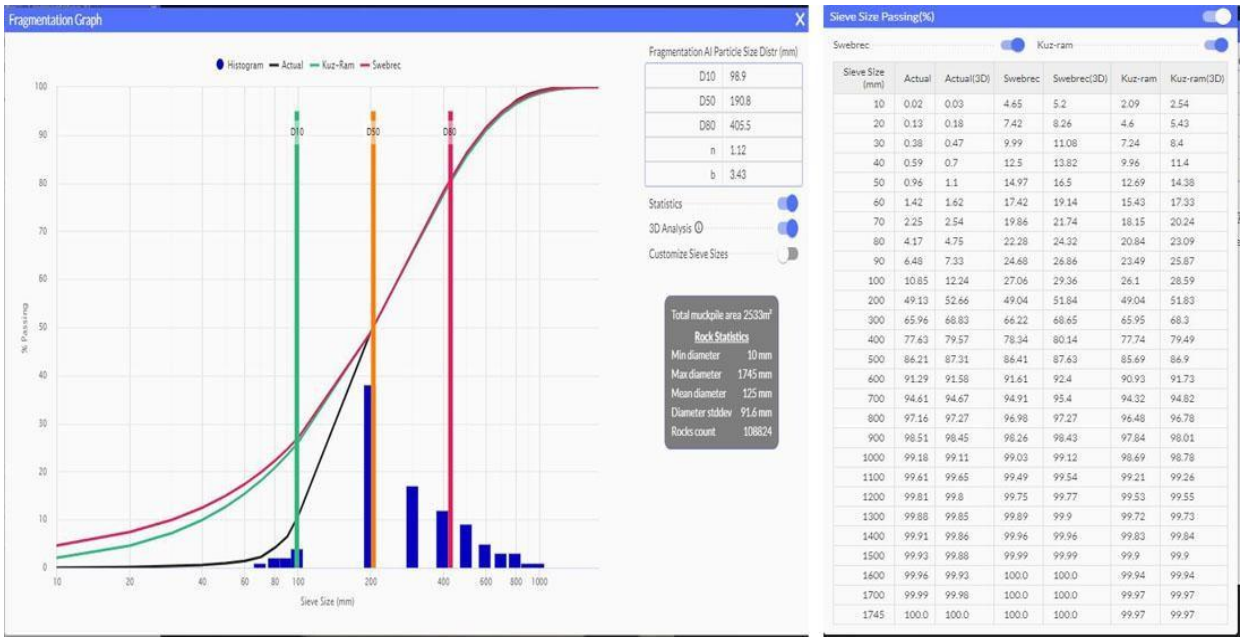

Sieve Size (mm)	Actual	Actual(3D)	Swebrec	Swebrec(3D)	Kuz-ram	Kuz-ram(3D)
10	0.02	0.03	4.65	5.2	2.09	2.54
20	0.13	0.18	7.42	8.26	4.6	5.43
30	0.38	0.47	9.99	11.08	7.24	8.4
40	0.59	0.7	12.5	13.82	9.96	11.4
50	0.96	1.1	14.97	16.5	12.69	14.38
60	1.42	1.62	17.42	19.14	15.43	17.33
70	2.25	2.54	19.86	21.74	18.15	20.24
80	4.17	4.75	22.28	24.32	20.84	23.09
90	6.48	7.33	24.68	26.86	23.49	25.87
100	10.85	12.24	27.06	29.36	26.1	28.59
200	49.13	52.66	49.04	51.84	49.04	51.83
300	65.96	68.83	66.22	68.65	65.95	68.3
400	77.63	79.57	78.34	80.14	77.74	79.49
500	86.21	87.31	86.41	87.63	85.69	86.9
600	91.29	91.58	91.61	92.4	90.93	91.73
700	94.61	94.67	94.91	95.4	94.32	94.82
800	97.16	97.27	96.98	97.27	96.48	96.78
900	98.51	98.45	98.26	98.43	97.84	98.01
1000	99.18	99.11	99.03	99.12	98.69	98.78
1100	99.61	99.65	99.49	99.54	99.21	99.26
1200	99.81	99.8	99.75	99.77	99.53	99.55
1300	99.88	99.85	99.89	99.9	99.72	99.73
1400	99.91	99.86	99.96	99.96	99.83	99.84
1500	99.93	99.88	99.99	99.99	99.9	99.9
1600	99.96	99.93	100.0	100.0	99.94	99.94
1700	99.99	99.98	100.0	100.0	99.97	99.97
1745	100.0	100.0	100.0	100.0	99.97	99.97

Figure 13. Fragmentation graphs and mean fragmentation sizes based on SWEBREC ,KUZRAM and actual.

This study adopted an advanced methodology for evaluating muck-pile geometry to improve measurement accuracy and reduce data-processing time. Key muck-pile parameters—namely drop, throw, and lateral dispersion—were determined using AI-driven algorithms applied to a three-dimensional model generated from UAV-acquired imagery. This integrated approach enhanced both the reliability and efficiency of the measurements.

The software platform allows users to interrogate specific sections of the reconstructed 3D model and accurately compute distances between any two points, including vertical elevation differences. By replacing conventional manual measurement techniques, this method significantly streamlines the assessment process while improving measurement precision. Representative iterations of the measured muck piles are illustrated in Figure 14(a–g).

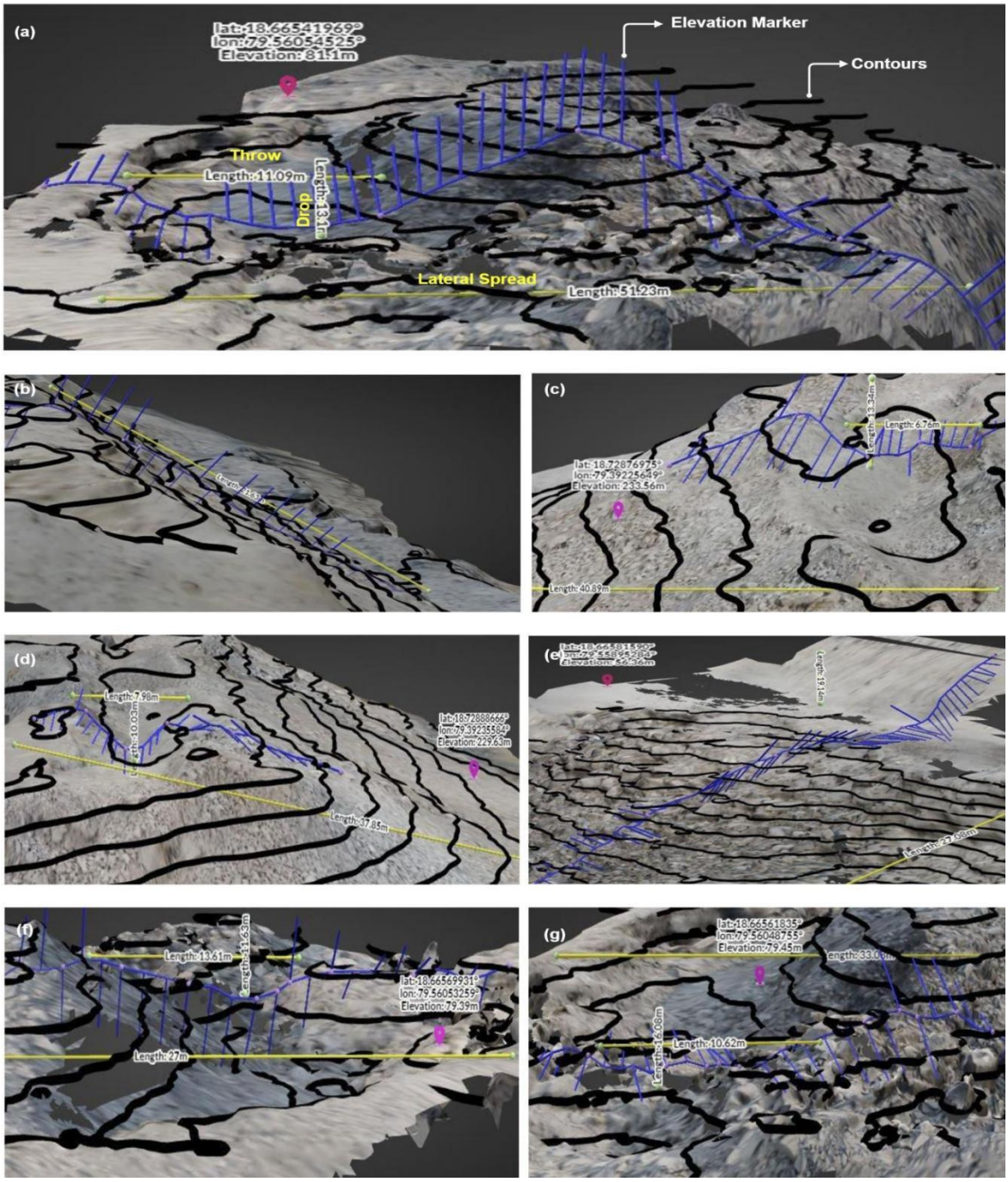

Figure 14. (a, b, c, d, e, f and g): Muck pile Characteristics; Throw, Drop, and lateral spread measurement in software using aerial photographs captured by UAV presented for few random blasts.

The AI framework utilizes a U-Net convolutional neural network to generate a flattened three-dimensional model of the bench, incorporating joint structures and visualizing the elevation profile of the muck pile fragments. Within the network, the convolutional layer serves as the initial processing stage, applying a filter (or kernel) that interacts with a localized region of input pixels, the size of which depends on the filter dimensions. This kernel performs operations beneficial for tasks such as edge detection, image sharpening, or blurring. As the kernel slides over the image, the element-wise multiplication of the filter values and corresponding pixel intensities is performed, and the results are summed to produce a single value, which is then propagated to subsequent convolutional layers. Following this, a max-pooling layer is applied to downsample the spatial dimensions of the feature maps, reducing the number of parameters and computational load within the network.

Table 3: Blast design parameters and results

Blast Design Parameters													Joint Features			Muckpile Characteristics		
S.No	Pattern	Phases	Blast No	No. rows	No Holes	Hole Diameter, mm	Average Hole Depth, m	Spacing Burden Ratio (Se/Be), m	Front Row Burden, m	Stemming Length, m	Average Explosive per hole, kg	Total Explosive, kg	Firing pattern	Joint Spanning Height,m	Joint Angle	Joint Set Number	Drop,m	Throw, m	Spread
Mine A																		
1	FP altered, All same	Phase - I	A1	3	30	150	12	1.3	2.5	4.5	390	11,700	1	1.5	70	1	7.7	2.3	12.3
2			A2	3	30	150	12	1.3	2.5	4.5		11.700	1	3.5	66	1	9	6.1	23.3
3			A3	3	23	150	12	1.3	2.5	4.5		8,655	1	3	53	1	11	5.3	15.3
4			A4	3	30	150	12	1.3	2.5	4.5		11,700	2	4	68	1	9	3.3	14.6
5			A5	3	28	150	12	1.3	2.5	4.5		10,460	2	4	32	1	12	4.1	13.4
6			A6	3	27	150	12	1.3	2.5	4.5		9,940	1	4.2	58	2	9	2.5	12.8
7			A7	3	30	150	12	1.3	2.5	4.5		11,700	3	3	90	2	5	1.6	13.8
8			A8	3	30	150	12	1.3	2.5	4.5		11,700	3	3.6	32	2	3	5.9	19.3
9	Se/Be Ratio altered, All same	Phase - II	B1	3	28	150	12	1.2	2.5	4.5	390	105460	1	1	53	2	6	2.5	14.6
10			B2	3	30	150	12	1.2	2.5	4.5		11,600	1	1.3	54	2	8	4.3	20.5
11			B3	3	28	150	12	1.2	2.5	4.5		10,450	1	3	62	3	4	3.1	12.8
12			B4	3	27	150	12	1.2	2.5	4.5		9,950	1	2.5	34	1	11	5.8	13.9
13			B5	3	28	150	12	1.3	2.5	4.5		10,700	1	1.4	32	2	12	2.1	14.2
14			B7	3	27	150	12	1.35	2.5	4.5		9,950	1	2.5	634	1	7	4.2	20.1
15			B6	3	27	150	12	1.3	2.5	4.5		9,700	1	2.7	45	1	5	5.8	13.1
16			B8	3	30	150	12	1.35	2.5	4.5		11,500	1	3.4	55	2	8	2.3	21.3
17	EQ &SL Altered, All same	Phase - III	C1	3	27	150	12	1.3	2.5	4.5	390	9,890	3	5.8	46	2	9	4.3	14.1
18			C2	3	30	150	12	1.3	2.5	4.5		11,800	3	4.6	75	2	7.5	5.7	22.1
19			C3	3	28	150	12	1.3	2.5	4.5		10,600	3	3.5	45	2	8	3.3	15.3
20			C4	3	27	150	12	1.3	2.5	5.5	325	7,020	3	2	90	2	5.8	2.4	23.5

21			C5	3	27	150	12	1.3	2.5	**5.5**		**8,775**	3	**3.1**	45	**2**	8	4.4	16.5
22			C6	3	30	150	12	1.3	2.5	**5.5**		**9,750**	3	**2**	47	**1**	5.7	5.6	17.9
23			C7	3	30	150	12	1.3	2.5	**6**		**11,780**	3	**4.72**	84	**2**	9	4.10	24.5
24			C8	3	27	150	12	1.3	2.5	**6**	292	**7,884**	3	**3.8**	52	**2**	7	5.11	26.5
25			C9	3	27	150	12	1.3	2.5	**6**		**7,860**	3	**2**	53	**2**	8.3	2.5	22.1
26			D1	3	27	150	12	1.3	2.5	4.5		**9,045**	2	**2.5**	65	**2**	7	4.5	15.3
27			D2	3	30	150	12	1.3	2.5	4.5	335	**9,756**	2	**2.9**	67	**2**	6.9	5.5	13.3
28			D3	3	26	150	12	1.3	2.5	4.5		**8,455**	2	**5.7**	72	**1**	9.3	3.4	12.6
29	EQ & DL Altered, All same	Phase - IV	D4	3	28	150	12	1.3	2.5	4.5		**7,280**	2	**4.8**	48	**1**	11	2.6	16.5
30			D5	3	27	150	12	1.3	2.5	4.5	257	**7,020**	2	**2**	73	**1**	12.5	3.7	17.6
31			D6	3	27	150	12	1.3	2.5	4.5		**5.670**	2	**3.7**	55	**2**	7.9	5.5	21.1
32			D7	3	27	150	12	1.3	2.5	4.5		**5,660**	2	**2**	59	**3**	9.2	2.7	15.4
33			D8	3	27	150	12	1.3	2.5	4.5	210	**5,655**	2	**2.1**	82	**1**	8	4.6	16.5
34			E1	3	27	150	12	**1.25**	2.5	4.5		12,555	1	**2**	53	**2**	6	5.4	22.3
35			E2	3	27	150	12	**1.25**	2.5	4.5		13, 950	1	**2**	65	**1**	5	2.6	20.9
36	FP & Se/Be ratio together altered, All Same		E3	3	30	150	12	**1.25**	2.5	4.5		12,560	1	**2.4**	62	**1**	5.9	3.8	21.9
37		Phase - V	E4	3	27	150	12	**1.35**	2.5	4.5	465	12,470	2	**2**	57	**3**	9.4	5.6	15.9
38			E5	3	27	150	12	**1.35**	2.5	4.5		12,400	2	**2.6**	58	**3**	8	4.7	14.7
39			E6	3	27	150	12	**1.35**	2.5	4.5		13,621	3	**1.4**	90	**3**	7.7	2.8	12.5
40			E7	3	27	150	12	**1.4**	2.5	4.5		12,500	3	**5.21**	32	**3**	8	3.8	21.8
41			E8	3	30	150	12	**1.4**	2.5	4.5		13.800	3	**6**	19	**3**	5.9	4.8	26.6
42			G1	3	26	150	12	1.3	2.5	4.5		**8,800**	**3**	**4.65**	**43**	**2**	**7**	**5.4**	**23.3**
43			G2	3	31	150	12	1.3	2.5	4.5	325	**9,830**	**3**	**2**	**26**	**3**	**6.9**	**2.9**	**21.3**
44	DL , EQ & FP altered, All same	Phase - VI	G3	3	25	150	12	1.3	2.5	4.5		**8,521**	**2**	**4**	**42**	**3**	**8**	**3.8**	**22.3**
45			G4	3	28	150	12	1.3	2.5	4.5	265	**7,255**	**2**	**2.3**	**47**	**3**	**8**	**4.5**	**18.6**
46			G5	3	27	150	12	1.3	2.5	4.5		**7,200**	**3**	**2**	**75**	**3**	**8**	**5.3**	**17.8**
47			G6	3	27	150	12	1.3	2.5	4.5	220	**5,940**	**1**	**2**	**71**	**3**	**6**	**2.10**	**12.4**
48			G7	3	27	150	12	1.3	2.5	4.5		**5,900**	**1**	**2.7**	**47**	**3**	**4**	**4.10**	**13.6**
									Mine B										
49			A17	3	30	150	12	1.3	2.5	4.5		4,200	**2**	**2.04**	**55**	**2**	**8.9**	**2.1**	**14.8**
50			A18	3	28	150	12	1.3	2.5	4.5		3,920	**2**	**5**	**41**	**2**	**6.8**	**4.5**	**15.8**
51	FP altered, All same		A19	3	27	150	12	1.3	2.5	4.5		3,780	**2**	**3**	**37**	**2**	**5**	**3.8**	**13.6**
52			A20	3	30	150	12	1.3	2.5	4.5	140	4,200	**1**	**3**	**84**	**3**	**8**	**5.4**	**12.8**
53		Phase - I	A21	3	28	150	12	1.3	2.5	4.5		3,820	**1**	**5.4**	**37**	**2**	**2.8**	**5.10**	**21.6**
54			A22	3	27	150	12	1.3	2.5	4.5		3, 800	**3**	**2.6**	**58**	**2**	**8**	**3.5**	**25.8**
55			A23	3	27	150	12	1.3	2.5	4.5		3, 790	**3**	**3.7**	**69**	**2**	**7.6**	**2.5**	**12.1**
56			A24	3	23	150	12	1.3	2.5	4.5		3,220	**3**	**4**	**55**	**3**	**8**	**4.6**	**15.5**
57	Se/Be Ratio altered,		B177	3	23	**150**	12	**1.2**	2.5	4.5		3,335	2	**4.3**	34	**3**	8	2.10	16.4
58		Phase - II	B18	3	28	150	12	**1.2**	2.5	4.5	145	4,060	2	**4**	63	**3**	8	3.2	21.6
59			B19	3	27	150	12	**1.2**	2.5	4.5		3,915	2	**1.2**	57	**2**	8.5	4.6	25.6
60			B20	3	27	150	12	**1.3**	2.5	4.5		3,900	2	**5**	65	**3**	5	5.10	21.8

61	All same		B21	3	30	150	12	**1.3**	2.5	4.5		4,350	2	**1.32**	45	**3**	5	2.8	12.6
62			B22	3	27	150	12	**1.3**	2.5	4.5		3,920	2	**5.34**	34	**3**	5	3.6	17.6
63			B23	3	27	150	12	**1.35**	2.5	4.5		3,932	2	**3**	65	**2**	5	2.4	13.4
64			B24	3	30	150	12	**1.35**	2.5	4.5		3,913	2	**3.12**	77	**3**	6	4.2	19.5
65			C19	3	28	150	12	1.3	2.5	**4.5**		**3,920**	1	**2**	65	**2**	3	5.5	19.3
66			C20	3	31	150	12	1.3	2.5	**4.5**	140	**4,340**	1	**2.4**	35	**3**	5	2.6	21.1
67			C21	3	30	150	12	1.3	2.5	**4.5**		**4,200**	1	**2.1**	44	**2**	5	3.1	20.5
68			C22	3	27	150	12	1.3	2.5	**5.5**	120	**3,960**	1	**3**	47	**2**	5	2.8	13.6
69	EO &SL	Phase - III	C23	3	28	150	12	1.3	2.5	**5.5**		**3,960**	1	**3**	85	**2**	5	4.7	20.6
70			C24	3	30	150	12	1.3	2.5	**6**		**4,320**	1	**4**	44	**2**	9	5.8	16.7
71			C25	3	30	150	12	1.3	2.5	**6**	110	**3,300**	1	**3**	37	**3**	9	2.4	14.8
72			C26	3	27	150	12	1.3	2.5	**6**		**2,970**	1	**1.1**	51	**2**	5.6	3.8	15.9
73			C27	3	27	150	12	1.3	2.5	**6**		**2,980**	1	**4.3**	57	**2**	6	4.9	12.9
74			D17	3	27	150	12	1.3	2.5	4.5		**2,700**	1	**4.1**	85	**2**	6	5.6	21.9
75			D18	3	30	150	12	1.3	2.5	4.5	100	**3,000**	1	**4**	44	**2**	6	2.1	20.3
76	EQ & DL Altered, All same	Phase - IV	D19	3	26	150	12	1.3	2.5	4.5		**2,600**	1	**1.5**	35	**2**	6.8	3.8	15.7
77			D20	3	28	150	12	1.3	2.5	4.5		**2,240**	1	**3.5**	64	**1**	9.4	5.3	13.4
78			D21	3	27	150	12	1.3	2.5	4.5	80	**2,160**	1	**3**	35	**1**	6	3.3	12.4
79			D22	3	26	150	12	1.3	2.5	4.5		**2,080**	1	**4**	75	**1**	6	4.8	23.5
80			D23	3	30	150	12	1.3	2.5	4.5	60	**1,800**	1	**2.4**	74	**1**	6	2.1	25.9
81			D24	3	27	150	12	1.3	2.5	4.5		**1,620**	1	**2**	34	**1**	6	5.9	13.6
82			E17	3	27	150	12	**1.25**	2.5	4.5		3,780	3	**2.6**	66	**1**	6	2.8	14.9
83	FP & Se/Be ratio together altered, All Same	Phase - V	E18	3	27	150	12	**1.25**	2.5	4.5		3,790	3	**1.4**	25	**1**	9	**2.10**	16.3
84			E19	3	30	150	12	**1.25**	2.5	4.5		4,200	3	**5.21**	37	**1**	9	**4.8**	17.8
85			E20	3	27	150	12	**1.35**	2.5	4.5	140	3,810	1	**6**	58	**1**	5.6	2.6	19.5
86			E21	3	30	150	12	**1.35**	2.5	4.5		4,210	1	**5.7**	64	**2**	6.3	3.5	25.4
87			E22	3	29	150	12	**1.35**	2.5	4.5		4,060	2	**5.32**	47	**2**	8	5.5	12.7
88			E23	3	27	150	12	**1.4**	2.5	4.5		3,800	2	**1**	85	**2**	6	4.6	13.4
90			E24	3	28	150	12	**1.4**	2.5	4.5		3,920	2	**3.2**	44	**2**	3	5.4	16.5
91			G15	3	26	150	12	1.3	2.5	4.5		**2,860**	**1**	**2**	**35**	**2**	**7**	**3.7**	**18.3**
92			G16	3	31	150	12	1.3	2.5	4.5	110	**3,410**	**1**	**2**	**78**	**2**	**9**	**5.3**	**17.5**
93	DL , EQ & FP altered, All same	Phase - VI	G17	3	30	150	12	1.3	2.5	4.5		**3,300**	**2**	**2.7**	**67**	**2**	**3**	**4.3**	**22.5**
94			G18	3	27	150	12	1.3	2.5	4.5		**2,700**	**2**	**3.2**	**90**	**2**	**6**	**2.5**	**25.3**
95			G19	3	30	150	12	1.3	2.5	4.5	100	**3,000**	**2**	**3.9**	**47**	**1**	**8.7**	**4.7**	**22**
96			G20	3	27	150	12	1.3	2.5	4.5		**2,430**	**3**	**2.7**	**88**	**2**	**9**	**3.8**	**15.6**
97			G21	3	26	150	12	1.3	2.5	4.5		**2,340**	**3**	**3.2**	**85**	**2**	**9**	**2.9**	**18**

3.5. Blast Geometry & Energetics

Across the experiments, the blast hole burden and spacing ranged 2.5 m and 3.0–3.5 m respectively, depending on joint direction and dipping plane alignment. The powder factor varied between 0.40 – 0.65 kg/m³ in coal benches using SME and 0.30 – 0.45 kg/m³ in limestone benches using ANFO. These design values were maintained constant in each experimental phase to isolate the impact of firing pattern, decking length, and S/B ratio.

4.0. Results & Discussions:

4.1. Impact of Firing Pattern on Muckpile Characteristics:

The results indicate in figure 15 that the V firing pattern achieves a drop of 3 meters, a throw of 5.9 meters, and a lateral spread of 19.3 meters, making it particularly effective for optimizing rock fragmentation and displacement. This pattern's perpendicular alignment to the free face allows for precise, controlled detonation timing, leading to ideal in-flight collisions among rock fragments. These dynamic breaks the rock into well-sized fragments, enhancing lateral spread while keeping vertical displacement to a minimum. The V pattern also reduces burden and increases spacing, resulting in less confinement around blast holes, enabling more effective lateral energy dissipation and controlled fragmentation. This minimizes excessive drop depths, producing a stable working surface that aids excavator efficiency, as the shallow 3-meter drop allows for easier access, reducing repositioning needs and streamlining loading cycles.

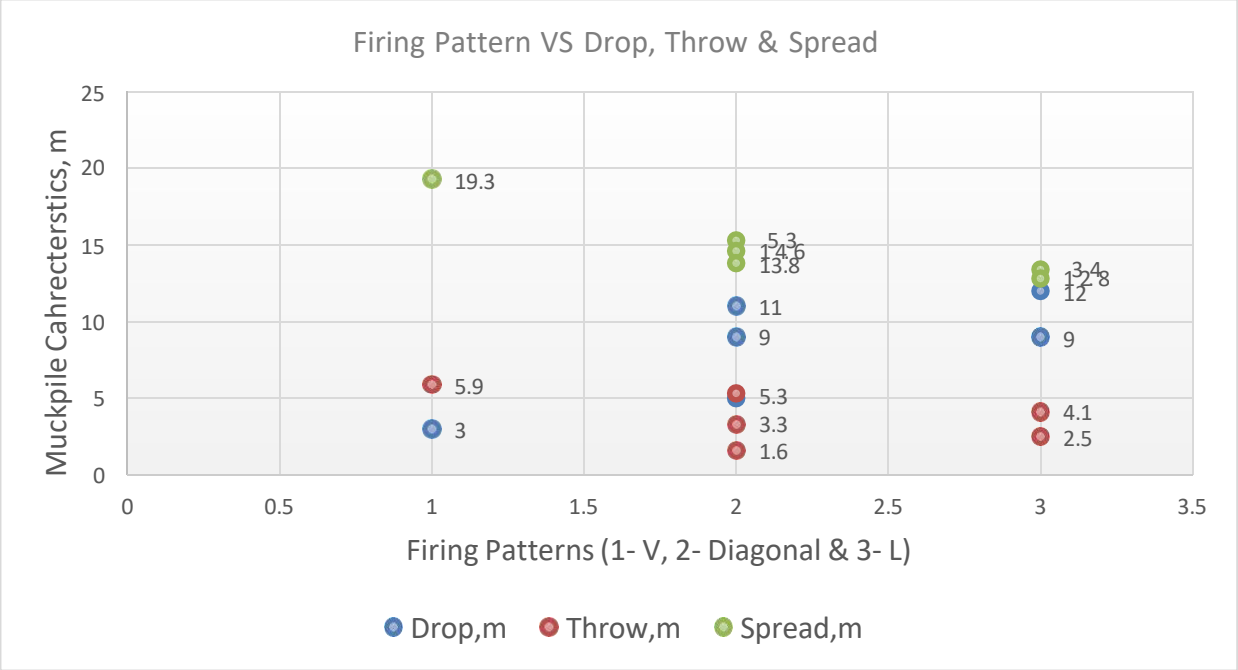

Figure 15: Relation between Firing Pattern and Muckpile Characteristics

In contrast, the diagonal firing pattern produced a deeper drop of 11 meters, a throw of 5.3 meters, and a lateral spread of 15 meters, while the line pattern resulted in a maximum drop of 12 meters, a throw of 4.1 meters, and a lateral spread of 13 meters. These configurations, with their oblique and linear firing sequences, direct more energy vertically, leading to deeper drop zones and limited lateral spread, which can hinder excavation and equipment mobility.

Overall, the V firing pattern proves to be the most effective choice when excavation efficiency and bench stability are key priorities.

4.2. Impact of Spacing Burden Ratio on Muckpile Characteristics:

The observed results with varying spacing-to-burden (S/B) ratios in figure 16 can be explained through energy distribution and rock fragmentation principles. A lower S/B ratio (1.2) concentrates explosive energy vertically, leading to a higher drop but reduced lateral spread and throw, limiting excavation efficiency. Increasing the ratio to 1.3 distributes energy more evenly, enhancing throw and lateral spread but causing an excessive vertical drop, which can lead to inefficiencies in excavation. In contrast, a ratio of 1.35 optimizes energy use by balancing vertical drop (around 5 meters) with enhanced lateral spread (21 meters), ensuring more effective rock fragmentation and displacement. This ratio reduces excessive drop,

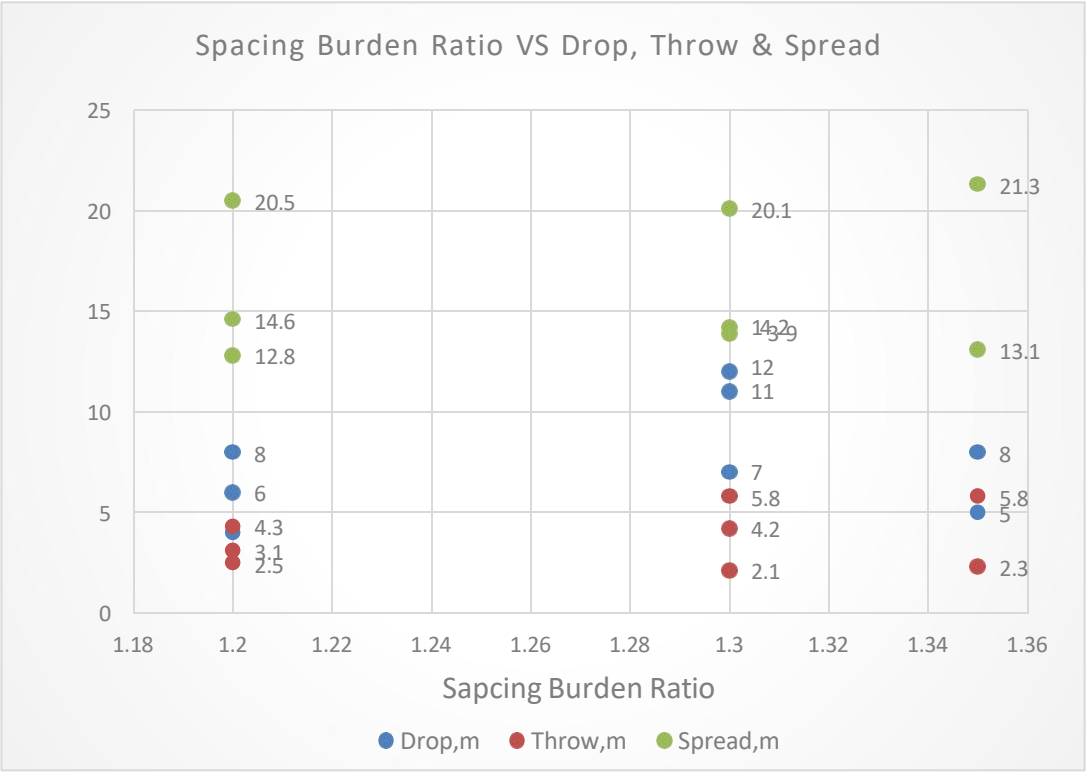

Figure 16: Relation between Spacing Burden Ratio and Muckpile Characteristics

Improving muck-pile stability and excavator performance, while maximizing lateral spread for better operational efficiency and reduced energy waste. The 1.35 S/B ratio thus provides a more effective and economical solution for blast design by maximizing horizontal displacement and optimizing vertical fragmentation, leading to improved overall productivity.

4.3. Impact of Decking Length on Muckpile Characteristics:

Decking length influence as shown in figure 17, which refers to the distance between explosive charges in a blast hole, plays a crucial role in how energy is distributed throughout the rock mass. When the decking length is shorter, such as 1 meter, the explosive energy is concentrated over a smaller vertical

zone, resulting in a more controlled release of energy and leading to an optimal vertical drop (10 meters), horizontal throw (5 meters), and lateral spread (15 meters). Shorter decking lengths allow for better coupling between adjacent charge sections, enhancing vertical fragmentation and creating a stable muck-pile for easier excavation. As the decking length increases to 1.5 meters and 2 meters, the energy is spread over a larger vertical distance, which increases the drop (12 meters at 1.5 meters and 5 meters at 2 meters), throw (6 meters at 1.5 meters and 14 meters at 2 meters), and lateral spread (16 meters at 1.5 meters and 22 meters at 2 meters).

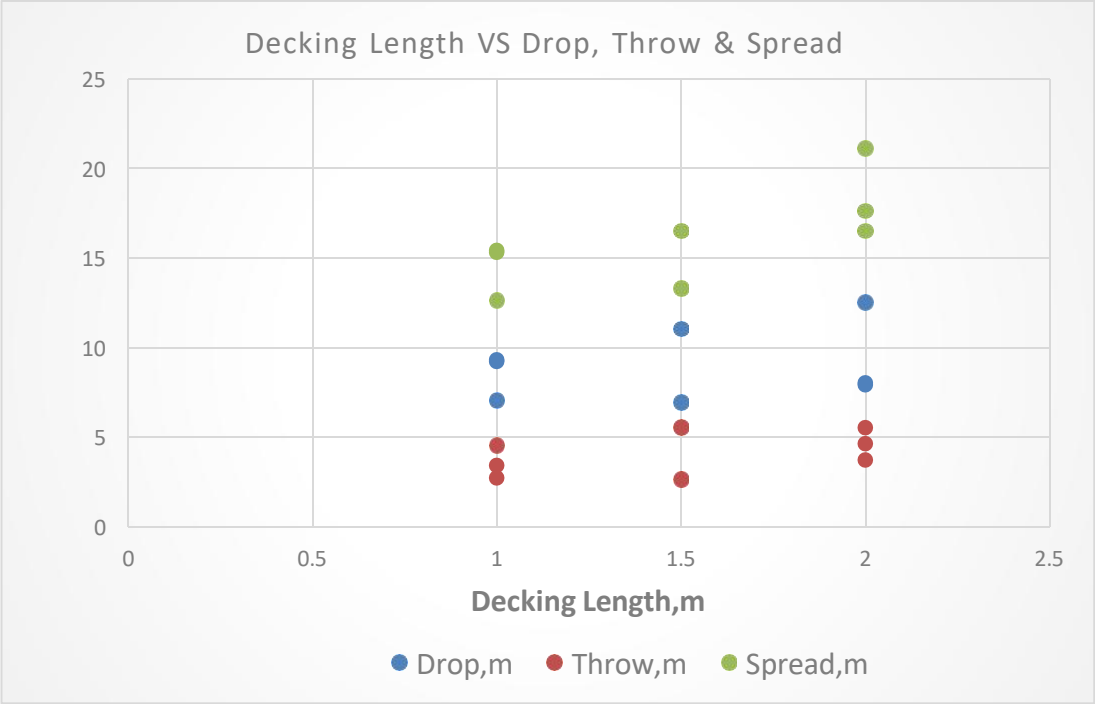

Figure 17: Relation between Decking Length and Muckpile Characteristics

However, the larger decking length reduces the coupling between charges, causing excessive horizontal energy distribution and increasing lateral spread at the cost of reduced vertical fragmentation. The 1-meter decking length achieves a finer balance of both vertical and horizontal energy distribution, ensuring efficient fragmentation and a stable muck-pile, while longer decking lengths, despite enhanced lateral spread and throw, reduce overall blast efficiency for excavation due to less effective vertical fragmentation.

4.4. Impact of Cumulative Impact of V Firing Pattern, Spacing Burden Ratio and Decking Length on on Muckpile Characteristics:

The observed optimal muck-pile characteristics in figure 18, including reduced drop, controlled throw, and enhanced lateral spread, can be explained through the principles of explosive energy distribution and rock fragmentation dynamics. A decking length of 1 meter allows for a more concentrated release of explosive energy over a shorter vertical distance, ensuring better coupling between charge sections. This concentration of energy in a controlled vertical zone leads to a more efficient rock fragmentation, resulting in a smaller drop of less than 4 meters. The reduced drop minimize the creation of oversized fragments and reduces the risk of unstable muck-piles, enhancing excavation efficiency.

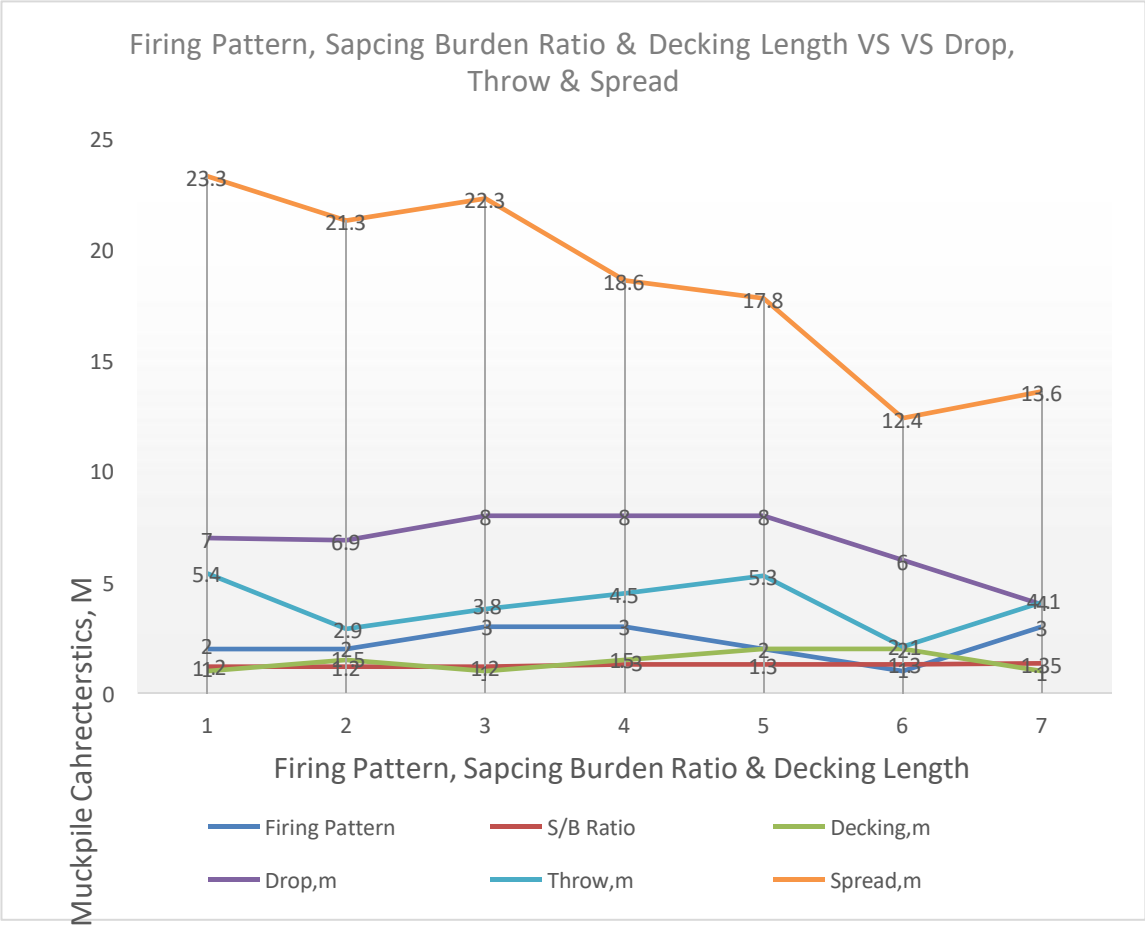

Figure 18: Relation between Combination Blast Design Parameters and Muckpile Characteristics

A spacing-to-burden ratio of 1.35 further optimizes energy distribution by ensuring that explosive energy is effectively shared between the vertical and horizontal directions, leading to a balanced lateral spread of more than 15 meters. This ratio prevents excessive vertical energy dissipation, ensuring effective horizontal displacement while maintaining control over fragmentation. The V- shaped firing pattern optimizes the directional energy release, which enhances lateral spread while minimizing excessive throw. This pattern ensures that the energy is directed efficiently, creating a muck-pile that is both stable and well-distributed, making it ideal for excavation and loading with shovels. Together, these parameters result in a blast that is both safe and economical, providing optimal fragmentation and reducing the need for secondary blasting while improving operational efficiency.

5. Conclusion:

- In this study, UAVs played a crucial role in capturing high-quality muck-pile photographs, which were essential for characterizing key blast results such as drop, throw, and lateral spread. Principal Component Analysis (PCA), performed using XLSTAT, was instrumental in identifying and selecting the most influential blast design parameters affecting the blast outcomes.

- AI tool was effectively used to design blasts based on insights derived from the baseline study and PCA results

- A special AI tool within Strayos software was also utilized, which is unique in its ability to characterize key blast parameters, including throw, drop, and lateral spread.

- The results from this study unequivocally demonstrate that the **V-firing pattern** is the optimal choice for controlled rock fragmentation and efficient excavation. This results in well-sized fragments with a 3-meter drop, 5.9-meter throw, and 19.3-meter lateral spread, improving muck-pile stability and operational efficiency.

- The **spacing-to-burden ratio** of 1.35 optimizes energy distribution, balancing vertical drop (5 meters) with enhanced lateral spread (21 meters). This ratio reduces vertical energy dissipation, improving fragmentation and operational efficiency.

- A **decking length of 1 meter** further enhances performance by concentrating explosive energy in a smaller vertical zone, ensuring controlled fragmentation and a stable muck-pile.

- These findings underline the importance of combining the V-firing pattern, spacing-to-burden ratio of 1.35, and 1m short decking lengths to achieve the most efficient and economical blast design. Such an approach not only improves excavation efficiency but also contributes to the economic viability of the operation by minimizing the need for secondary blasting and optimizing loading cycles. The reduced vertical drop and enhanced lateral spread allow for efficient rock displacement, improving the overall productivity of the mining operation and reducing the operational costs associated with excavation and loading.

- Future research will focus on expanding the methodology to deeper benches and different rock types, integrating real-time blast monitoring, and developing AI-based decision tools capable of predicting muck-pile characteristics prior to blasting at mine-wide scale. This will enable continuous optimization of blasting operations, allowing dynamic adjustment of design parameters to further enhance productivity and sustainability in mining operations.

Authors contribution

All authors are contributed equally.

Data availability

Data will be available on reasonable request from the corresponding authors.

Conflicts of interest

The authors declare no conflict of interest.

Ethical statement

Authors state that the research was conducted according to ethical standards.

Funding body

This research received no external funding.

References

[1] Choudhary, B. S. (2019). Effect of blast induced rock fragmentation and muckpile angle on excavator performance in surface mines. *Mining of Mineral Deposits*, *13*(3), 119-126.

[2] Zou, D., & Zou, D. (2017). Explosives. *Theory and Technology of Rock Excavation for Civil Engineering*, 105-170.

[3] Xu, P., Yang, R., Zuo, J., Ding, C., Chen, C., Guo, Y., ... & Zhang, Y. (2022). Research progress of the fundamental theory and technology of rock blasting. *International Journal of Minerals, Metallurgy and Materials*, *29*(4), 705-716.

[4] Ouchterlony, F. (2003). Influence of blasting on the size distribution and properties of muckpile fagments: a state-of-the-art review.

[5] Liu, Q., Shi, F., Wang, X., & Zhao, M. (2022). Statistical Estimation of Blast Fragmentation by Applying 3D Laser Scanning to Muck Pile. *Shock and Vibration*, *2022*.

[6] Brunton, I., Thornton, D., Hodson, R., & Sprott, D. (2003). Impact of blast fragmentation on hydraulic excavator dig time. Fifth Large Open Pit Mining Conference, 39-48.

[7] Monjezi, M., Rezaei, M., & Yazdian Varjani, A. (2009). Prediction of rock fragmentation due to blasting in Gol-E-Gohar iron mine using fuzzy logic. *International Journal of Rock Mechanics and Mining Sciences, 46*(8), 1273–1280. https://doi.org/10.1016/j.ijrmms.2009.05.005

[8] Rai, P. (2002). Evaluation of effect of some blast design parameters on fragmentation in open cast mine. Ph.D. thesis, Banaras Hindu University, Varanasi.

[9] McKenzie, C.K. (1999). A review of the influence of gas pressure on block stability duringrockblasting, Procs. Explo-99, Kalgoorlie, WA, pp: 173-179.

[10] Stagg, M.S., Otterness, R.&Siskind, D.F.(1992).Effects of blasting practices on fragmentation ,Rock Mechanics, Titherson Ed., Balkema, Rotterdam, pp:313-322. 33rd U.S. Symposium on Rock Mechanics (USRMS), Santa Fe, New Mexico, June 1992. Paper Number: ARMA-92-0313 Published: June 03.

[11] Adamson,W.R., Scherpenisse,C.R.& Diaz,J.C.(1999).The use of blast monitoring modeling technology for the optimization of development blasting, Proc.Explo-99,Kalgoolie,WA, pp: 35-41.

[12] Kanchibotla,S.S.,Valery,W.&Morrell,S.(1999).Modelling fines in blast fragmentation and its impact on crushing and grinding,Procs.Explo-99,Kalgoorlie,WesternAustralia, pp: 137-144.

[13] Monjezi, M., & Rezaei, M. (2011). Developing a new fuzzy model to predict burden from rock geomechanical properties. *Expert Systems with Applications, 38*(8), 9266–9273. https://doi.org/10.1016/j.eswa.2011.01.029

[14] Rezaei, M., Monjezi, M., Ghorbani Moghaddam, S. *et al.* Burden prediction in blasting operation using rock geomechanical properties. *Arab J Geosci* **5**, 1031–1037 (2012). https://doi.org/10.1007/s12517-010-0269-0

[15] Sri N. Chandrahas, B.S. Choudhary, N.S.R. Krishna Prasad,V. Musunuri, K.K. Rao, An Investigation into the Effect of Rockmass Properties on Mean Fragmentation. Arch. Min. Sci. 2021, 66, 561–578.

[16] N. S. Chandrahas, B. S. Choudhary, and M. S. Venkataramayya, "Competitive algorithm to balance and predict blasting outcomes using measured field data sets," *Computers & Geosciences*, vol. 27, pp. 1087–1110, 2023. [Online]. Available: https://doi.org/10.1007/s10596-023-10254-x

[17] M. Naresh, N. S. Sri Chandrahas, G. Praful Kumar, et al., "Harmonizing blasting efficiency: A case study on evaluation and optimization of fragmentation size and ground vibration," *Journal of the Institution of Engineers (India): Series D*, 2024. [Online]. Available: https://doi.org/10.1007/s40033-024-00730-8

[18] Rezaei, M., Monjezi, M., Matinpoor, F., Mohammadi Bolbanabad, S., & Habibi, H. (2023). Simulation of induced flyrock due to open-pit blasting using the PCA–CART hybrid modeling. *Simulation Modelling Practice and Theory, 129*, 102844. https://doi.org/10.1016/j.simpat.2023.102844

[19] Cunningham, C.V.B. (1987) Fragmentation Estimations and the Kuz-Ram Model—Four Years on. In: Fourney, W.L. and Dick, R.D., Eds., Second International Symposium on Rock Fragmentation by Blasting, Keystone, Colorado, Bethel CT: SEM, 475-487.

[20] Pradeep, T., Chandrahas, N. S., & Fissha, Y. (2024). A Principal Component-Enhanced Neural Network Framework for Forecasting Blast-Induced Ground Vibrations. J. Civ. Hydraul. Eng., 2(4), 206-219. https://doi.org/10.56578/jche020402

[21] N. S. Chandrahas, Y. Fissha, B. S. Choudhary, B. Olamide Taiwo, M. S. Venkataramayya, and T. Adachi, "Experimental data-driven algorithm to predict muckpile characteristics in jointed overburden bench using unmanned aerial vehicle and AI tools," *International Journal of Mining, Reclamation and Environment*, pp. 1–35, 2024. https://doi.org/10.1080/17480930.2024.2340876

[22] Chandrahas, N.S., Choudhary, B.S., Venkataramayya, M.S. *et al.* An Inventive Approach for Simultaneous Prediction of Mean Fragmentation Size and Peak Particle Velocity Using Futuristic Datasets Through Improved Techniques of Genetic XG Boost Algorithm. *Mining, Metallurgy & Exploration* **41**, 2391–2405 (2024). https://doi.org/10.1007/s42461-024-01045-8.

[23] Sri Chandrahas; Bhanwar Singh Choudhary; MS Venkataramayya; Yewuhalashet Fissha; Blessing Olamide Taiwo. "An investigation of the cumulative impact of decking length and firing pattern on blasting results", *Journal of Mining and Environment* , 2024, -. doi: 10.22044/jme.2024.14555.2743.

[24] N. S. Chandrahas, B. S. Choudhary, M. S. Venkataramayya, Y. Fissha, and N. R. Cheepurupalli, "AI-driven analysis of rock fragmentation: The influence of explosive charge quantity," Acadlore Trans. Geosci., vol. 3, no. 3, pp. 123–134, 2024. https://doi.org/10.56578/atg030301.

[25] Chiappetta, R.F., Borg, D.G. & Sterner, V.A. (1987). Explosives and rock blasting. Atlas Powder Company,Dallas, pp:233.

[26] Frimpong, M., Kabongo, K., & Davies, C. (1996). Diggability in a measure of dragline effectiveness and productivity. Proceedings of the 22nd Annual Conference on Explosives and Blasting Techniques, 95-104.

[27] Abd Elwahab, A., Topal, E., & Jang, H. D. (2023). Review of machine learning application in mine blasting. *Arabian Journal of Geosciences*, *16*(2), 133.

[28] Rajwar, K., Deep, K., & Das, S. (2023). An exhaustive review of the metaheuristic algorithms for search and optimization: taxonomy, applications, and open challenges. *Artificial Intelligence Review*, 1-71.

[29] Lee, K. S., & Geem, Z. W. (2005). A new meta-heuristic algorithm for continuous engineering optimization: harmony search theory and practice. *Computer methods in applied mechanics and engineering*, *194*(36-38), 3902-3933.

[30] Desale, S., Rasool, A., Andhale, S., & Rane, P. (2015). Heuristic and meta-heuristic algorithms and their relevance to the real world: a survey. *Int. J. Comput. Eng. Res. Trends*, *351*(5), 2349-7084.

[31] Zhang, S., Ma, X., & Yan, J. (2018). Effects of Blast Design Parameters on Fragmentation in an Open Pit Mine. Mining, Metallurgy & Exploration, 35(3), 415-425.

[32] Bhandari, S. (1975). Burden and Spacing Relationship in the Design of Blasting pattern. 16th Symp. Rock Mechanics, University of Minnesota, pp 333-343

[33] Sandeep Prasad, B.S. Choudhary, A.K. Mishra. Effect of Blast Design Parameters on Blast Induced Rock Fragmentation Size – A Case Study. Int. Conf. on Deep Excavation, Energy Resources and Production DEEP16 24-26 January 2017, IIT Kharagpur, India

[34] Smith,N.S.(1976). An investigation of the effects of blast hole confinement on generation of ground vibration in bench blasting, Final report for blasting research, SMI grant section, p.301.

[35] Zhang, Z. X., Qiao, Y., Chi, L. Y., & Hou, D. F. (2021). Experimental study of rock fragmentation under different stemming conditions in model blasting. *International Journal of Rock Mechanics and Mining Sciences*, *143*, 104797.

[36] Wu, Q., Huang, Y., & Tang, C. (2019). Effects of Joint Spacing on Rock Fragmentation and Muck Pile Characteristics in Open-Pit Mining. Minerals, 9(9), 554.

[37] Chen, Q., Zhang, Y., & Shi, X. (2017). Influence of Joint Orientation on Muck Pile Fragmentation under Blasting. International Journal of Mining Science and Technology, 27(5), 833-838.

[38] Cundall, P.A. (1990). Numerical modelling of jointed and faulted rock. In: Rossmanith HP (ed) Mechanics of jointed and faulted rock. A.A. Balkema, Rotterdam.

[39] Belland, J.M. (1968). Structure as a Control in Rock Fragmentation Coal Lake Iron Ore Deposited. The Canadian Mining and Metallurgical Bulletin. 59 (647), 323-328.

[40] Li, Q., Liu, S., & Wang, Y. (2021). Effects of Bedding Plane Orientation on Particle Size Distribution and Shape of Muck Pile Fragmentation. Advances in Civil Engineering, 2021, 6651309.